SANDIA REPORT
SAND2001-1665
Unlimited Release
Printed August 2001

Solder Joint Reliability Predictions for Leadless Chip Resistors, Chip Capacitors, and Ferrite Chip Inductors Using the SRS™ Software

Paul T. Vianco and Steven N. Burchett

Prepared by
Sandia National Laboratories
Albuquerque, New Mexico 87185 and Livermore, California 94550

Sandia is a multiprogram laboratory operated by Sandia Corporation, a Lockheed Martin Company, for the United States Department of Energy under Contract DE-AC04-94AL85000.

Issued by Sandia National Laboratories, operated for the United States Department of Energy by Sandia Corporation.

Available to DOE and DOE contractors from
U.S. Department of Energy
Office of Scientific and Technical Information
P.O. Box 62
Oak Ridge, TN 37831

Telephone: (865)576-8401
Facsimile: (865)576-5728
E-Mail: reports@adonis.osti.gov
Online ordering: http://www.doe.gov/bridge

Available to the public from
U.S. Department of Commerce
National Technical Information Service
5285 Port Royal Rd
Springfield, VA 22161

Telephone: (800)553-6847
Facsimile: (703)605-6900
E-Mail: orders@ntis.fedworld.gov
Online order: http://www.ntis.gov/ordering.htm

SAND2001-1665
Unlimited Release
Printed August 2001

Solder Joint Reliability Predictions for Leadless Chip Resistors, Chip Capacitors, and Ferrite Chip Inductors Using the SRS™ Software

Paul T. Vianco
Tribology, Mechanics, and Melting Department

Steven N. Burchett
Solid Mechanics Engineering Department

Sandia National Laboratories
P.O. Box 5800
Albuquerque, NM 87185

Abstract

The SRS™ software provided reliability predictions regarding the thermal mechanical fatigue (TMF) failure of solder joints for three sizes of chip resistor, three sizes of chip capacitor, as well as three sizes and three material compositions of ferrite chip components (inductors) assembled on a laminate printed wiring board. Four "use" conditions and one accelerated testing condition were assessed using an end-of-life failure rate criterion of 10 ppm for the service conditions and an 50% end-of-life failure rate after accelerated testing. The chip resistors and capacitors would provide reliable electrical functionality over the entire product lifetime. Significant TMF in the gap location would reduce the mechanical strength of the joints. The ferrite components would also provide reliable electrical functionality over the entire product lifetime. A lower joint strength would be expected in some of the joints due TMF in the gap location. The accelerated test conditions were predicted to cause a decrease in mechanical strength for the resistor, capacitor, and ferrite component solder joints, more so in the case of the resistors and capacitors and to a lesser degree for the ferrite devices, due to TMF in the solder joint gap locations. However, a predicted absence of TMF failure in the solder joint fillets would result in, no catastrophic loss of mechanical integrity or the loss of electrical performance to the solder interconnects of the devices.

Introduction

Satellite application

The long-term reliability of a Global Positioning System (GPS) satellite is strongly dependent upon the uninterrupted operation of on-board electronic systems. In turn, the continuous operation of satellite electronics is governed by the reliability of solder interconnects. Because satellite repair is often cost-prohibitive, the solder interconnects must be highly reliable. It is preferred that the aging-related degradation of solder joints be predicted at the product design stage in order to assure that the hardware meet the desired service lifetime.

The primary aging mechanism in surface mount solder interconnects is that of thermal mechanical fatigue (TMF). Thermal mechanical fatigue degradation is caused by temperature fluctuations during the service cycle of the product. Such temperature variations introduce cyclic mechanical loads into the solder joints as a result of the mismatch in thermal expansion coefficients between the chip material, the solder, and the circuit board (laminate). Those cyclic loads introduce deformation into the solder microstructure. The continuous build-up of deformation culminates into the formation of micro-cracks and subsequently, a continuous crack that causes electrical and/or mechanical failure of the solder interconnect.

A GPS application was identified that would include surface mount technology circuit boards in its electronic package. The circuit boards would be populated with, amongst other devices, several configurations of leadless chip resistors, capacitors, and ferrite inductors. *Quantitative* solder joint reliability data for the selected sizes of chip components, the circuit board laminate, and "use" conditions were not available. Specifically, the circuit board functions necessitated the use of several chip components having relatively large dimensions. Only qualitative guidelines were obtained from a number of unpublished sources[1, 2, 3]. Therefore, a study was undertaken, the goal of which was to determine the reliability of solder joints for resistors, capacitor, and ferrite components used in this GPS application.

Methodology

The development of a reliability database for the ferrite, capacitor and resistor chip components began with identifying: (1) the particular environments that the electronics would experience in service as well as (2) the conditions that would be used in the accelerated testing program. Then, failure rate limits were determined for both use and accelerated testing conditions.

The service life of the satellite hardware included three stages: (1) manufacturing, (2) storage, and (3) the use condition representing actual flight. An underlying principle of TMF in solder joints is that damage is cumulative and largely independent of the prior history of the microstructure at the start of aging (Miner's rule). Therefore, fatigue damage caused by manufacturing processes and pre-flight storage is simply added to that incurred during the use condition. The thermal cycling parameters that described the manufacturing and storage conditions are listed in Table 1. The manufacturing segment

is described by a fixed number of cycles, 200. The specified temperature spread was 60C°; the low temperature limit was assumed to be 20°C; therefore, the high temperature limit was set at 80°C. It was assumed that a reasonable dwell time at the temperature limits would be 60 min. Storage conditions were specified with a temperature range of 6C°; the temperature limits were assumed to be17°C and 23°C, values which encompassed the 20°C baseline. The temperature variations occurred with a cycle time of 1 day (1440 min); thus, the hold times were 12 hours or 720 minutes (which assumes a negligible temperature ramp). Because pre-flight storage can approach 10 years for some hardware, the fixed number of cycles equal to 3650 (1 cycle/day x 365 days/year x 10 years) was used.

Four possible use conditions were identified for flight by the satellite electronics. These conditions are listed in Table 2. Three of the four conditions ("B,", "C,", and "D") were based upon a ΔT equal to 30C°. The fourth condition ("A"), which had the temperature limits of 20°C and 55°C for a ΔT equal to 35C°, was identified by the IPC-SM-785 and IPC-SM-9701 documents as representing conditions during geo-synchronous earth orbit [4, 5]. It was established that the satellite electronics would require a service life of 15 years. A geo-synchronous orbit would result in a 12 hour period between hot (exposed to the sun) and cold (behind the earth). Therefore, the dwell time at the temperature limits would be 12 hours, or 720 minutes. Assuming that the time required for the heat-up and cool-down processes is negligible, the solder joints would be exposed to 5475 cycles over the course of 15 years use lifetime.

The IPC-SM-785 document also stated a risk specification of 0.001% or 10 ppm failures at the end of the field life of the product. Therefore, a limiting value of 10 ppm was designated as the maximum failure rate for the solder interconnects at the end-of-life. The computed reliability results, specifically, the end-of-life failure rates, would be compared against this benchmark.

Besides the use environments to which the actual product would be exposed, an accelerated aging environment was also defined for the laboratory testing of solder joint reliability. The recommended cycle was identified in the IPC-SM-785 specification. The temperature limits were 0°C and 100°C. The dwell times at those limits was 15 min; a nominal ramp rate between limits was 10°C/min. This schedule would result in 28.8 cycles/day. The anticipated test duration was three months, which would allow for a total of 2520 cycles to be performed on the test vehicles

Next, the methodology used to assess the solder joint reliability for the resistor, capacitor, and ferrite components included two computational approaches. The first technique, the results of which form the basis of this report, determined an overall reliability for the surface mount joints using commercially available software - Solder Reliability Solutions™ 1.1, or SRS™ 1.1[6]. This software computes the solder joint failure statistics based upon the inelastic strain energy that accumulates in the solder joint during TMF. It was construed that once the solder joint had reached a particular level of inelastic strain energy, the interconnect was considered to have failed. The inelastic strain energy failure criterion was established from an extensive database of accelerated

aging experiment results that included a variety of surface mount package configurations[7, 8]. The inelastic strain energy metric for TFM is applied to a library of surface mount package configurations (e.g., leadless chip devices, gull-winged SOIC's, etc.). Parameters such as the specific package type and configuration as well as the thermal expansion coefficient and elastic modulus of both the chip and circuit board laminate materials are inputs into the model. The properties of the 63Sn-37Pb solder are already included in the soft ware. It is important to understand that this model predicts the reliability performance of the solder joint as a whole and thus, is an excellent screening tool for identifying potential trouble spots in terms of selected materials, solder joint configuration, or use condition. The SRS™ model does not quantify the extent of damage at specific locations within the solder joint. Nor is the SRS software sufficiently flexible to addresses package configurations that deviate significantly from those contained in the software library.

In the event that the SRS software indicates a situation of potentially low reliability for one or more of the components, a second, more exacting, 3-D model developed at SNL would be engaged. This latter model would use a more detailed constitutive equation for Sn-Pb solder as well as finite element analysis to predict deformation in Sn-Pb solder at any location within the interconnect. Since the finite element analysis is computationally intensive, its use should be limited to only those critical cases identified by the SRS™ assessments as requiring further evaluation.

Geometries and materials

Components

Three sizes were evaluated for each of the chip resistor, chip capacitor, and ferrite components. The nomenclatures used to identify the component sizes were: (1) 1206, 2010, and 2512 chip resistors; (2) 1210, 1812, and 1825 chip capacitors; and (3) 0805, 1206, and 1806 ferrite components. Shown in Fig. 1 is a schematic diagram showing the chip device dimensions that were pertinent to the reliability calculations. The corresponding dimensions for each of the resistor, capacitor, and ferrite components are listed in Table 3. The dimensional specification provided for each component in Table 3 are a nominal value that represents a potential range of size[9]. The dimensions of the ferrite components were provided by K. Olsberg, SNL[10].

The chip resistor material was alumina. Because the actual resistive element on top of the alumina chip is very thin, it would not cause the elastic or thermal expansion properties of the chip to deviate significantly from those of alumina. The coefficient of thermal expansion and elastic modulus properties used in the reliability calculations were those provided directly by the SRS™ software: a coefficient of thermal expansion equal to 6×10^{-6} °C^{-1} and an elastic modulus of 53×10^{6} psi (tension and flexure). Although the precise composition of the alumina was not revealed, these values, which are in excellent agreement with literature data, were utilized for all temperature ranges as designated for in the manufacturing, storage, and use conditions[11]. The alumina material properties were also used to represent chip capacitors, albeit, capacitor material is typically not alumina. However, in the absence of a resource for the parameters of

actual chip capacitor material, the alumina properties would serve as a suitably conservative approximation.

The availability of the elastic modulus and thermal expansion coefficient properties was severely limited for the ferrite components to be used in this study. There existed a modest data base of ferrite thermal expansion coefficient data at SNL as well as in the literature[12, 13]. However, both references confirmed that the expansion coefficient vary considerably between different ferrite compositions. A similar situation would likely prevail for the elastic modulus property. Because of the uncertainty in identifying the appropriate properties for the ferrite materials to be used in this product, it was decided to measure the thermal expansion coefficient and elastic moduli directly on bulk material from the Fair-Rite Corp., the company which would supply the actual inductor components.

Three Fair-Rite material compositions were identified for potential use in the ferrite chips for this application: #43 (Y material), #61 (Z material), and #73 (X material). These compositions were immediately available in a manufacturers "sample" kit; the kit also included the commonly used #65 composition for which the coefficient of thermal expansion was evaluated, as well. The material samples were in a cylindrical geometry having lengths that ranged from 0.4300 to 0.4500 in. At the same time, discussions with Fair-Rite engineers culminated in they providing us with samples of each of the #43, #61, and #73 materials having a rectangular geometry: 0.500±0.001 in. (length) x 0.250 in. (width) x 0.250 in. (thickness). Coefficient of thermal expansion measurements were performed on both the cylindrical ("kit") samples as well as the specially constructed rectangular samples. There was no significant difference in the coefficient values between the cylinder ("kit") material and the newly processed rectangular material. Also, due to the availability of testing resources used to measure the elastic modulus, these latter data were completed only on the rectangular materials. *In light of testing logistic and the need to expedite project completion, the reliability calculations were performed using the coefficient of thermal expansion values from the "kit" (cylindrical) materials and the elastic parameters measured for the specially made rectangular samples.*

The thermal expansion coefficient was measured using the dialotometry technique. Besides acquiring the expansion coefficient, this test technique also allowed for the identification of any phase changes in the material as a function of temperature. It is important to be aware of such phase changes since they are often accompanied by changes to the thermal expansion and elastic modulus properties that that are used in the solder joint reliability calculations. The tests were performed over a temperature range between –50°C and 200°C. The data was outputted as sample length as a function of temperature. When compared to the original length of the specimen, l_o, the changes to the specimen length were sufficiently small so as to permit a calculation of the dimensionless length change, $\Delta l/l_o$. Thus, the coefficient of thermal expansion coefficient (CTE) was defined as:

$$CTE = (\Delta l/l_o)/ \Delta T(C°) \qquad (1)$$

It was stated above that there was not a significant difference in the coefficient of thermal expansion between the cylindrical ("kit") samples and the specially constructed rectangular specimens. This point is illustrated in Table 4a which shows the coefficient of thermal expansion that was calculated over 25C° temperature intervals, beginning at –50°C and ending at 200°C. The data show the often-observed, general trend in which the coefficient increases at higher temperatures. Thermal expansion measurements were also made on four other specimens, three of which, were actual ferrite chip devices. The Fair-Rite #65 material was evaluated; it was tested only in the cylindrical geometry (from kit II, having a length of 0.2518 in.). The three chip capacitors were designated: (1) BUM41PO312 (0.1754 in.), (2) 257T612 (0.1800 in.), and (3) 257X111 ("low speed" material, 0.1275 in.). Expansion measurements on the actual ferrite chip devices were prone to be slightly more noisy due to their reduced size. The coefficient values for these four materials appear in Table 4b.

The thermal expansion curves were examined for pronounced variations in the respective elongation plots; such abnormalities would indicated possible phase transitions in the materials. The #73 showed a slight peak in the plot for both cylindrical and rectangular samples; the peak occurred in the range of 0-25°C. The #43 material showed a similar peak at the same temperature location, but with only the cylindrical specimen. The #65 material (of which there was only the cylindrical geometry) also exhibited a small peak in the 0-25°C range. The reversibility of these artifacts was not verified by performing a cool-down step and subsequently, examining the thermal *contraction* behaviors. Nevertheless, the effects of this peak on the coefficient of thermal expansion were of the order of the absolute error of the measurement/computational techniques used to obtain the thermal expansion coefficient values. Moreover, in the case of the #73 material, the mechanism behind the thermal expansion peak did not affect the elastic properties of the samples. In summary, the small peak in the 0-25°C temperature range that was observed in several of the plots of thermal expansion versus temperature, whatever their source, did not significantly impact either the thermal expansion or elastic modulus properties of any of the compositions.

The coefficient of thermal expansion values for the ferrite materials were determined for temperature ranges that were specific to each of the manufacturing, storage and use environments as outlined in Tables 1 and 2. The temperature ranges and coefficient of thermal expansion values (again, representing the cylindrical ("kit") materials) are listed in Table 5.

The elastic properties were obtained for the three materials: #43, #61, and #73 (rectangular specimens) using the acoustic technique. The procedure uses the velocity of sound waves in the material to compute the following elastic properties: Young's (elastic) modulus, shear modulus, bulk modulus, and Poisson's ratio. In order to compute these parameters, the density of the ferrite materials was required. The buoyancy method (methanol bath) was used to determine the density values. Resources permitted density measurements to be performed only at 25°C. Over the limited temperature range of interest, the changes in density were considered very small; therefore, a single value was

used over the various temperature intervals. The densities of the cylindrical and rectangular materials are shown in Table 6. Two samples were evaluated per case. The worst-case difference between the two samples was approximately 4%. The elastic moduli designated for each of the duty cycles and material types have been listed in Table 7. It is apparent from the data in Table 7 that the elastic modulus did not change significantly with temperature; this observation was true of all of the elastic properties measured for the ferrite materials.

Printed circuit board

The printed circuit board material was a high glass transition temperature (170°C) FR-4 glass epoxy laminate. The circuit board was 0.052 in. thick. The board design included six Cu layers (two surface layers and four internal layers); the circuit board was also to be conformal coated after solder assembly. The coefficient of thermal expansion is particularly sensitive to the composition of the circuit board laminate in terms of epoxy and glass content, the weave of the laminate, and the Cu layers. The elastic properties tend to be less sensitive to these parameters. I would be best practice to determine the expansion behavior of each vendor-lot of the circuit board laminate. However, it is understood that such measures were presently impractical. Therefore, the coefficient of thermal expansion, as well as the elastic moduli (tension and flexure) used in the reliability calculations, were those provided in the SRS™ software library. Those values are: a coefficient of thermal expansion of 18×10^{-6} °C^{-1}; an elastic (tension) modulus of 4.1×10^{6} psi; and a flexure modulus of 2.8×10^{6} psi.

Several assumptions require clarification. First of all, it was assumed that the Cu internal layers would not impact the properties. The coefficient of thermal expansion parameter for Cu is 17×10^{-6} °C^{-1}, which is comparable to that of the laminate structure (specifically, the epoxy)[14]. On the other hand, the Cu layers will raise the apparent elastic modulus of the laminate. The effect of a stiffer board on solder joint reliability is somewhat more difficult to predict, qualitatively. For example, while a stiffer board will cause more of the thermal expansion mismatch strains to be accommodated as inelastic strain in the solder joints, a decrease in laminate curvature will, in turn, reduce the degree of deformation introduced into the solder microstructure.

The second assumption was that the conformal coating (nominally 0.003 in. thick) would not have a significant impact on the TMF performance of the solder joints. Such a presumption has been readily utilized by other investigators. The assumption has generated little to no opposition from the electronics community because conformal coating layers are sufficiently thin and compliant (<0.010 in.) as to have minimal impact on the board, device, or solder joint response to the temperature fluctuations.

A generalized schematic diagram of the circuit board land (pad) pattern to which the chip components would be soldered, is shown in Fig. 2. The dimensions of the lands corresponding to the specific resistor, capacitor, and ferrite components are listed in Table 8.

Reliability computation - set-up

The reliability computation was performed for each of the three resistor and three capacitor sizes as well as for each of the three ferrite sizes and three material varieties (#43, #61, and #73), per geometry. Thermal mechanical fatigue deformation, followed by subsequent crack generation and propagation (damage), occur along the pathway shown in Fig. 3a. The shear strain per cycle is highest in the gap region of the joint. The shear strains in the gap location have two contributions: (1) the *global* strains due to thermal expansion mismatch between the chip package and the printed wiring board and (2) the *local* strains due to the thermal expansion mismatch between the solder and the chip package as well as between the solder and the printed wiring board. Both global and local thermal expansion mismatch strains are inversely proportional to the gap width; smaller gaps lead to larger strains and a faster TMF damage build-up in the solder. The actual site of crack initiation may be any where in the gap; however, it is typically at the inside edge of the solder pad (under the component) because a small stress concentration develops there due to the abrupt geometry change there. Although the mechanical strength of the joint has been compromised by cracking within the gap region, the interconnect maintains electrical functionality due to the intact fillet. The geometry of the interconnect, as it is used in the SRS™ reliability calculation *for the gap region of the joint*, is shown in Fig. 3b. The *distance to the neutral point, or DNP,* was taken from the center of the chip device to the center of the termination on the bottom of the device.

Once the gap region has been damaged, cracking then appears in the fillet location. Once a crack has propagated completely through the fillet, electrical failure ensues. The same mechanisms of global and local shear strain are active for TMF of the solder in the fillet. However, it is apparent that the "gap" between the chip device and printed circuit board, which defines the extent of such deformation is much greater in the fillet than under the device. Hence, TMF processes are sharply curtailed in the fillet, thereby prolonging the fatigue life of the overall interconnect. In fact, the reliability of a chip device solder joint is determined primarily by the extent of TMF deformation/damage occurring in the fillet region.

Based upon the premise that shear deformation is responsible for TMF in the solder joint fillet location, the reliability computation requires that an effective gap be defined for the fillet. Experiments have shown that, in general, a crack propagates through the fillet at an angle of approximately 45°. The schematic diagram in Fig. 3c shows the crack path in the fillet. An effective gap was defined for the shear strain computation. First, an effective fillet height, H', was set equal to D, the distance from the edge of the package to the outboard edge of the pad. This methodology assumes that complete wetting/spreading to the pad edge of the pad has taken place. Therefore, the distance of crack propagation is x and the area of cracking is x multiplied by the width of the device or pad, which ever is the smaller. The value of x was computed from the pad geometry and D; the expression for x is $D/\sqrt{2}$. An effective gap was defined as the separation distance between the vertical face of the chip termination and the pad at the midpoint of the crack path (x/2). Therefore, the gap thickness is 2(x/2) or simply the dimension, x. The DNP for the fillet was computed as the distance from the chip center location to the point half-way along the crack path, as the latter is projected onto the pad.

At this point, an analysis was made as to whether TMF processes in the gap and those in the fillet occur serially or whether they occur in parallel with one-another. In the event that they are serial in nature, the overall reliability of the solder joints would be based upon a simple addition of the cycles-to-failure from the two locations. In the latter case, the geometry, gap or fillet, having the greater number of cycles-to-failure would govern the device reliability. *It was assumed that TMF in the gap and fillet locations of the joint occur in parallel*. That is, the deformation in the fillet occurred at the same time as did TMF in the gap location.

An additional stipulation of the parallelism between TMF in the fillet versus that in the gap was that the two TMF processes were independent. First of all, the relatively low modulus and yield strength of the solder suggests that solder in each of the gap and fillet locations causes a negligible constraint on the respective expansion/contraction of the chip device and printed circuit board. Thus, the loss of solder integrity within the gap would not significantly affect the loads being placed on the solder in the fillet (or the reverse if such were the case.

A second basis regarding the independence of TMF processes between the gap and fillet regions addresses crack propagation. Generally speaking, microstructural damage that supports the formation of a continuous (large scale crack) occurs simultaneously throughout the gap length (Fig. 3b), beginning as microcracks which then grow and combine together to form the continuous crack. In a number of instances, cracking appears to initiate at, and propagate from, the in-board edge of the pad. That phenomenon arises from the fact that a small stress concentration is present at the pad edge due to the material/geometry discontinuity. Then cracking, like the stress concentration, moves along the already, heavily deformed gap region, towards the fillet. However, it is the extensive TMF deformation/damage that has already occurred in the gap region, which then supports the growth of the continuous crack.

A similar situation describes TMF of solder in the fillet. That is, TMF deformation/damage develops in the fillet primarily on the basis of the shear strain present there (albeit, those shear strains are not as homogenous in the fillet as they are in the gap location). The arrival of the "gap" crack at the fillet (i.e., at the bottom corner of the chip device) causes a small stress enhancement above that which is already present there due to the change in geometry and proportion of materials. Again, although that added stress concentration may guide the initiation of the continuous crack, by-and-large, it is the TMF deformation/damage that has already developed which determines the progress of the continuous crack toward the fillet surface.

In summary, TMF, and its associated deformation and damage (microcracking) processes, occurs in each of the gap and fillet locations, independently of one or the other location. And, at each location, it is the TMF deformation/damage that is, by far, responsible for the subsequent progress of a continuous crack. Because TMF occurs independently in the gap and fillet locations, the resulting parallelism of the TMF process between the two locations implies that the reliability of the electrical performance of the

interconnects is determined by that location (gap or fillet) that has the greater number-of-cycles to failure. *That location is the solder joint fillet*.

However, the mechanical strength of the solder joints will depend upon the extent of TMF processes in *both* the gap and fillet locations. The strength of the solder joints may be an important property with respect to the types of shock and vibration loads imposed on the devices during transportation and flight.; hence, the TMF reliability of gap location was computed for all of the components. Unfortunately, the thickness of the gap under chip devices, a critical parameter for determining the magnitude of TMF, is not easily controlled. Some factors include pad and termination geometries, the surface tension of the molten solder (which is significantly affected by the flux), the weight of the chip, and most importantly, the soldering process. Although some preliminary SRS™ reliability calculations were performed on the resistor and capacitor components have gaps that ranged from 0.001 in. to 0.005 in., past experience had shown that a *gap thickness of 0.001 in.* would most likely be expected for the range of chip components used in the present study.

It was noted above that the life cycle of the satellite electronics included, not only the use condition of service in space, but also the manufacturing process (e.g., multiple assembly steps requiring elevated temperatures, burn-in steps, etc.) as well as the storage environment that the product would experience prior to it being placed into orbit. The fact that the solder joints will have already been exposed to TMF as a result of the manufacture and storage segments implies that the interconnects would not begin their use condition in an "as-fabricated" state. Although TMF that occurs in the various stages are additive (Miner's rule), it is advantageous to represent the TMF cycles that occur in manufacture and storage segments, as "use condition" cycles. In this way, the effective "use condition" cycles generated in the manufacture and storage segments, can be directly subtracted from the actual use condition cycles to indicate remaining fatigue life. For example, in the case of the chip resistor and capacitor analyses, the failure-rate-at-end-of-life (2P Weibull) calculated by the software did, in fact, take into account the reliability loss during the use condition due to the manufacturing and storage segments.

On the other hand, the software calculates the number of cycles required to reach a failure rate F per each individual segment. That is, the reliability loss due to manufacture and storage was not introduced into the computation of the cycles-to-failure rate F for the particular use condition. However, it was important to know the number of use condition cycles remaining after taking into account the effects of manufacturing and storage, that would lead up to the specified failure rate.

A similar situation prevailed for the 3P Weibull analyses. In the case of the chip resistors and capacitors, the failure free time parameter was, in fact, computed for a use condition by taking into account the cumulative effects of manufacturing and storage segments. However, the cycles-to-first failure, $N_{o,i}$, is outputted only for the individual segments, that is, manufacture, storage, *or* use condition. In this latter case, it would be necessary to compute a reduced value of $N_{o,i}$ for the use conditions that reflects the TMF effects of the manufacturing and storage segments that preceded it.

Finally, in the case of the ferrite devices, *all* of the reliability calculations pertained only to individual segments: manufacture, storage, *or* use conditions. This situation arose because each of the manufacture, storage, and use conditions required separate calculations due to material properties of the ferrite materials changed with the respective temperature ranges. As in the case of the resistors and capacitors, it was preferable to calculate a reliability lifetime that included the cumulative effects of manufacturing and storage conditions.

It was clear from the above discussions that a methodology was needed with which the TMF that takes place during the manufacturing and storage segments could be reflected in the reliability statistics of the use conditions for each of the resistor, capacitor, and ferrite components. In order to develop such a computations, it was necessary to identify a correlation between the TMF deformation/damage that occurs in the manufacturing and/or storage segments of the joint lifetime and the TMF deformation/damage that is inherent to the use condition. *That correlation was made through the total inelastic strain energy (SE_{total}) parameter*. Geometrically, the total inelastic strain energy is the area within the fatigue (or cyclic) hysteresis loop. Quantitatively, the total inelastic strain energy is a *scalar* metric of the extent of TMF deformation/damage that has been incurred by the solder microstructure within the joint. The adjective, "total," means that the inelastic strain energy which is being considered, reflects the thermal expansion mismatch strains generated by both global (SE_{global}) and local(SE_{local}) effects.

The procedure for developing the inelastic strain energy correlation is described below. First, the total inelastic strain energy per cycle ($SE_{total, mfg}$) was documented from the SRS™ output for the manufacture segment. The amount of total inelastic stain energy accumulated in the manufacturing segment is simply ($SE_{total, mfg}$) times 200 cycles. Similarly, the total inelastic strain energy per cycle was downloaded from the software output for the storage segment ($SE_{total, storage}$). The amount of total inelastic stain energy accumulated in the storage segment is simply ($SE_{total, storage}$) times 3650 cycles. Next, the inelastic strain energy per cycle was documented from the SRS™ output for the particular use condition ($SE_{total, use}$). Therefore, the manufacturing segment represents an equivalent number of use condition cycles calculated from the expression:

$$N_{mfg \rightarrow use} = \left[(SE_{total, mfg}) \times 200\right] / (SE_{total, use}) \quad (2)$$

Similarly, the storage segment is equivalent to the number of use condition cycles calculated by equation (3):

$$N_{storage \rightarrow use} = \left[(SE_{total, storage}) \times 3650\right] / (SE_{total, use}) \quad (3)$$

The effective use cycles calculated for the manufacturing and storage segments were then subtracted from the stand-alone, use condition cycles to give the number of remaining use

condition cycles which do not exceed the specified failure rate. Those remaining use cycles were termed the "cumulative effect" use cycles. This approach was used on both 2P Weibull and 3P Weibull reliability data.

Using a similar approach, the 2P Weibull, "cumulative effect" *failure rate,* $\underline{F}$*,* could be calculated from the 2P Weibull, use condition failure rate, F, that is calculated by the SRS™ software. First, it was designated that a failure rate of F can be expected after $N_f(F) = 5475$ cycles of a particular use condition. The total inelastic strain energy analysis outline above then determined that the manufacturing and storage segments together were equivalent to N' cycles of the particular use condition as follows:

$$N' = N_{mfg \rightarrow use} + N_{storage \rightarrow use} \tag{4}$$

The entire lifetime of the solder joints, which includes manufacturing, storage, and use, can be represented by an equivalent number of use cycles, $\underline{N}_f(\underline{F})$, that is equal to:

$$\underline{N}_f(\underline{F}) = N_f(F) + N' \tag{5}$$

In mathematical form, the 2P Weibull distribution failure rate is represented by the following equation:

$$F(N_f) = 1 - \exp\left\{-[N_f/\alpha]^{\beta}\right\} \tag{6a}$$

where α is the number of cycles representing the characteristic life (F = 63%) and β is the slope parameter, $\beta = 4.0$. Solving for $N_f(F)$, the following expression was derived:

$$N_f(F) = \alpha\left[-\ln(1-F)\right]^{1/\beta} \tag{6b}$$

The failure rate, $\underline{F}$, was computed by taking the ratio of $N_f(F)/\underline{N}_f(\underline{F})$, which eliminates the need for an expressed value for α; the simplified equation follows:

$$\underline{F}(\underline{N}_f) = 1 - \exp\left\{[\underline{N}_f/N_f(F)]^{\beta}\ln(1-F)\right\} \tag{7}$$

In summary, equation (7) provides the means to compute the 2P Weibull, "cumulative effect" failure rate $\underline{F}(\underline{N}_f)$ that would be observed upon completion of the manufacture, storage, and the particular use condition.

It is necessary to review several details of the 2P Weibull reliability calculations as they are performed by the SRS™ software. As was shown in equation (4a), the 2P Weibull distribution has two descriptive parameters: (1) the characteristic life, α, and (2) the shape parameter, β. The characteristic life is often defined as the number of cycles responsible for a 1/e, or approximately, a 63% failure rate. In the case of the SRS™ software application, a similar user-defined input parameter was the failure rate at the end of life. A failure rate of 10 ppm was used in the present study for satellite service[4]. In

the case of accelerated testing conditions, a 50% failure rate was stipulated. The shape parameter, or slope β, was taken as 4.0 as this value was deem acceptable for good quality, leadless surface mount solder joints[4, 8].

The three-parameter, or 3P, Weibull distribution uses the same two parameters as were used in the 2P Weibull distribution, plus an added parameter, the failure free time, N_o. The expression for the 3P Weibull distribution is shown as equation (8) below:

$$F(N_f) = 1 - \exp\left\{-\left[(N_f - N_{o,i})/(\alpha - N_{o,i})\right]^{\beta}\right\} \qquad (8)$$

In the SRS™ software, the characteristic life, α, is not explicitly inputted; rather, the input parameter is the ratio of the failure-free time to the characteristic life; a value of 0.5 was selected for the present study. The 3P Weibull slope is not a user-defined parameter in the course of operating the software. It was assumed that the value of β was equal to 2.2 as is cited in the supporting literature[8].

The SRS™ software output for the 3P Weibull analyses is comprised of the cycles-to-first failure, $N_{o,i}$, and the failure free time. A computation was performed which determined the *3P failure rate at the end of life, F(N),* using equation (8) in order to make a direct comparison between the 2P and 3P Weibull predictions. In the absence of experimental data to determine the characteristic life, α, the 2P Weibull analysis was used to compute α for a failure rate of 63%. The computation of the "cumulative effects" values for the 3P Weibull parameters such as N_o; N_f, cycles to end-of-life; and $F(N_f)$, failure rate at the end-of-life, would use the same procedures as were described above for the 2P Weibull distribution case.

Finally, in general, the 3P Weibull distribution is considered to provide a better prediction of the wear-out degradation of solder joints in leadless ceramic packages, particularly at reduced cycle counts which would characterize the current study[8]. *Therefore, the reliability assessment of the resistor, capacitor, and ferrite component solder joints will be based upon the 3P Weibull computations*. The 2P Weibull reliability predictions which provide a conservative or lower limit reliability estimate were also computed.

Results and Discussion

Reliability computations for use (service) conditions

Leadless chip resistors and capacitors

The SRS™ software was exercised to determine the reliability of the chip resistor and chip capacitor packages under the four listed use conditions. Those computations were performed for the solder joint gap (0.001 in. thick), that forms between the chip termination and the circuit board pad, and for the solder joint fillet. The reliability data were calculated for both the 2P and 3P Weibull methodologies. Initially, some added emphasis will be placed on the 2P Weibull results in order to benchmark the output of the SRS™ model as well as to describe the physical reasons behind a number of qualitative trends. However, as noted above, the "accepted" life predictions will be based upon the 3P Weibull calculations.

The reliability predictions from the 2P Weibull analyses of the gap and fillet locations are presented in Tables 10 and 11, respectively. Two reliability metrics were documented. The first metric was the number of cycles N_f to reach an end-of-life failure rate equal to 10 ppm. This metric was calculated for *each* of the individual segments of the product life, that is, the manufacturing, storage, and either one of the four use conditions. The second metric was the failure rate at the end of life, $F(N_f)$. The end of life came after the 200^{th} cycle in the manufacturing segment; after the 3650^{th} cycle of the storage segment, or after the 5475^{th} cycle of the use condition. However, the SRS™ software computed an end-of-life failure rate value of the use condition that was based upon the "cumulative effect" of the manufacturing and storage segments that preceded it.

First, the reliability predictions for the resistors will be evaluated. The 2P Weibull results presented in Table 10 indicated that significant TMF could be expected in the gap region of the joints. First, it is observed that the 200 cycles of the manufacturing segment alone would exceed the number of cycles required to cause a product failure rate of 10 ppm in the gap location of all of the capacitor and resistor solder joints. By comparison, the 3650 temperature cycles representing the storage segment (17°C – 23°C) were well below the cycle counts required to reach a 10 ppm failure rate for that environment.

Turning to the four use conditions, the 5475 cycles (15 years) exceeded the number of cycles predicted to cause a 10 ppm failure rate, in some cases, by several orders of magnitude. The least amount of damage for the resistor solder joints, per the "cumulative effect" failure rates (in red), was observed with the 1206 geometry where the failure rates were between 1.2% and 76%. There was no significant difference in the reliabilities of the larger 2010 and 2512 resistors, each exhibiting nearly 100% end-of-life failures predicted for the gap location. In all but one case, that being the 1206 geometry under use condition "B", the global thermal expansion mismatch strains accounted for 90% to 100% of TMF deformation/damage in the solder joints. The fact that the gap location of the 1206 resistor exhibited the least TMF was attributed to its small length which, in turn, minimized the global thermal expansion mismatch strains in the solder. The 2010 and 2512 packages shared nearly identical cycles-to-failure (10 ppm) per use condition because the 2512 resistor has a greater crack area which compensated for the greater TMF degradation arising from it being nearly 20% longer than its 2010 counterpart.

The use conditions in Table 10 (and for that matter, similar tables presented later on) were listed in the order: "B," "C," "A," and "D." This order ranks the nominal temperature ranges from colder to warmer. It is observed in Table 10 that, for the chip resistors, the cycles required to reach the 10 ppm failure rate decreased in the order of conditions "B" to "C" and lastly, "A". Likewise, the "cumulative effect" failure rates increased in the same order of use conditions. The source of these trends over use conditions "B" through "A" was the fact that the increasingly greater nominal temperatures resulted in increasingly greater amounts of TMF in the gap as more inelastic (creep) deformation was introduced into the solder. An improvement in reliability between use conditions "A" and "D" was likely caused by the drop in the elastic modulus

of the solder, thereby allowing it to accommodate more of the thermal expansion mismatch through elastic rather than inelastic deformation.

The reliability predictions for the gap locations of the chip capacitors will be similarly examined. An interesting observation that was made at the beginning of the capacitor analysis was the fact that the reliability of the 1210 capacitor solder joint (gap) was poorer than that of the 1206 resistor, in spite of both being represented by the same material; both components having similar lengths; and the capacitor even having the advantage of a greater joint area over which fatigue cracks would be required to propagate. This apparent discrepancy was reconciled by the fact that the 1210 capacitor had a greater body thickness as compared to the resistor (see Table 3). A similar line-of-reasoning explains the higher reliability that is predicted for the 2010 resistor versus the 1812 capacitor package. The reliability of the leadless chip solder joints (gap location) is degraded as the height (or thickness) of the chip body becomes greater, because an increased separation between expansion/contraction centerline of the chip and that of the circuit boards increases the likelihood of bending moments being introduced into the structure. Such bending moments most often magnify the thermal expansion mismatch strains introduced into the solder joint.

As was the case with the resistors, the number of cycles required to reach a 10 ppm failure rate in the gap location of the capacitor solder joints during the manufacturing segment were well below the 200 cycles that comprised that segment. Therefore, significant failures would have already occurred prior to the units being introduced into storage and subsequent service. The storage condition would have had a minimal effect on the reliability.

The gap location of the 1210 and 1812 capacitor solder joints were predicted to have100% failure rates at the end-of-life for all use conditions. Although the reliability of the solder joint gap for the 1825 capacitor did not reach 100% failure at the end of life, it clearly exceeded the F = 10 ppm level. The thermal expansion mismatch strains were 97% to 99% global in nature. The highest reliability was realized with the “B” use condition; the lowest was observed with the “A” condition; the “C” and “D” use conditions exhibited very similar, intermediate reliability levels between the first two levels.

Summarizing the data presented in Table 10, it is evident that the 2P Weibull analysis predicts significant TMF damage in the solder contained in the gap regions of the solder joints for both chip resistors and capacitors. In fact, the specified failure rate of 10 ppm was predicted to be exceeded in the manufacturing cycle, alone, prior to the product being placed into service.

The 2P Weibull reliability predictions for the fillet location of the chip resistor and capacitor solder joints are shown in Table 11. Unlike the gap location, the 200 manufacturing cycles (and 3650 storage cycles, for that matter) were well below the number of cycles that were predicted to cause a 10 ppm failure rate for all part geometries. An interesting observation from the chip resistor data in Table 11 was that

TMF damage decreased as the chip length increased. This trend was a consequence of the fact that the fillet dimensions and hence, fatigue life, were dependent upon the height and width dimensions of the components. For example, the 1206 resistors had relatively small fillets due to a limited height and width. Therefore, the area that is able to sustain crack propagation was correspondingly small. On the other hand, the 2010 and 2512 resistors had increasingly larger fillets which required larger areas to be cracked, thus increasing the TMF reliability of these component sizes. With the exception of the 1206 chip resistor exposed to use condition "A," the "cumulative effect" failure rates at the end of life (15 years, or 5475 cycles, of service) did not surpass the10 ppm limit.

The reliability predictions between the three chip capacitors showed that the longest fatigue life belonged to the largest package, the 1825 capacitor, owing to its large fillet dimensions. The lowest fatigue life was predicted for the 1812 capacitor. In only one instance did the "cumulative effect" end-of-life failure rate exceed the 10 ppm limit, that being the 1812 capacitor exposed to use condition "A."

Another interesting observation pertaining to the 2P Weibull reliability of the resistor and capacitor solder fillets was the fact that a significant amount of the inelastic deformation was local rather than global. The percentage of the strain being global dropped to 0 – 21% amongst the resistors; the values were higher for the capacitors at 30 – 60%, but well below the 97 – 99% values observed for the gap locations of either component type.

The ranking of the reliability of the solder joint fillets between the four use conditions was different than that observed for the gap location. In all but the case of the 1206 resistors, the use condition "D" was predicted to provide the longest solder fillet life. The ranking of the other use conditions in order of highest to lowest reliability were "B," "C," and "A," respectively; a similar order was observed for the gap locations (Table 10).

In summary, the 2P Weibull analyses applied to the fillet locations of the chip resistor and capacitor solder joints indicated that, in all cases except the 1206 resistor under use condition "A" and the 1812 capacitor with use condition "A", the failure rates did not exceed the reliability limit of 10 ppm. Fatigue damage in the fillet structures was not dependent explicitly upon the component length because the fillet size was dependent upon the ancillary dimensions of height and width for each of the components.

Next, the more critical 3P Weibull analyses were performed on the chip resistor and capacitor solder joints. The analyses began with the gap location; the reliability data are shown in Table 12. In the case of the manufacturing and storage segments, only the cycles to first failure were provided in the table. The number of manufacturing cycles predicted to reach first failure exceeded the 200 cycles characterizing this segment, albeit, by a somewhat limited margin in some cases. The 3650 cycles comprising the storage segment were well below the number of cycles needed to create a first failure.

Four reliability parameters were presented for each of the use conditions in Table 12. The first two parameters were (1) the cycles to first failure for the stand-alone use condition (bright blue) and below it, (2) the "cumulative effect" failure-free time for the

use condition (bright red). As noted earlier, these two parameters were direct outputs from the SRS™ software. The third and fourth parameters were (3) the "cumulative effect" cycles to first failure (dark blue) and (4) the "cumulative effect" failure rate at the end of the use condition which would be denoted F(N = 5475 use cycles) (dark red). The value of the "cumulative effect" cycles to first failure was calculated by multiplying "cumulative effect" failure free time (bright red) by 365 cycles/year; this approach was later confirmed by comparing the value calculated in this manner with that calculated by considering the effective number of use condition cycles represented by the inelastic strain energy accrued in the manufacturing and storage cycles. The "cumulative effect" failure rate at the end of life was calculated by means of equation (8). The value of α was computed from the 2P Weibull distribution for F(N) = 63%; the value of $N_{o,i}$ was the "cumulative effect" cycles to first failure (dark blue value in Table 12); and N was equal to the number of use condition cycles which was 5475.

As expected, in general, the reliability trends predicted by the 3P Weibull analysis of the gap location reflected those observed for the 2P Weibull analyses. Also, a comparison of the "cumulative effect" failure rate at the end of life values between the two distributions illustrates the reduced conservativeness of the 3P Weibull analysis as compared to the 2P Weibull computations (Table 10). Nevertheless, a review of the "cumulative effect" end-of-life failure rates in Table 12 (dark red) shows that the 3P Weibull distribution predicts such failure rates in the gap to exceed the 10 ppm limit in all but the case of the 1206 resistor used in condition "B." In a number of the combinations of device geometry and use condition, a 100% failure was predicted.

The results of the 3P Weibull analyses performed on the fillet locations of the chip resistor and capacitor solder joints are shown in Table 13. As in the case of the gap location, the overall trends predicted by the 3P Weibull distribution, as a function of part geometry and/or use condition, were similar to those predicted by the 2P Weibull distribution. The 200 manufacturing cycles and 3650 storage cycles were well below the number of cycles required to see a first failure. The 3P Weibull analysis predicted no failures of the resistor or capacitor component solder joint fillets over any of the four conditions.

In summary, the 2P Weibull and 3P Weibull analyses predicted similar trends in the reliability of the chip resistor and capacitor solder joints, gap and fillet locations, as a function of use condition. The 3P Weibull analyses was less conservative than the 2P Weibull counterparts. The following remarks will be limited to the 3P Weibull calculations based upon the "cumulative effect" of manufacturing, storage and use condition. The end-of-life (use condition) failure rates in the 0.001 in. thick solder joint gap was predicted to exceed the 10 ppm limit in all but the instance of a 1206 resistor under use condition, "B." In several cases, 100% failure rates were expected. At the solder joint fillet locations, the 3P Weibull analysis predicted no failures in all cases of resistor or capacitor package and any use condition. Therefore, the resistor and capacitor solder joints will sustain reliable electrical functionality over the manufacturing, storage, and potential use conditions of the product. A significant loss of mechanical strength can

be expected from all of the solder joints due to the prevalence of TMF damage in the gap locations.

Ferrite devices

The results of the 2P Weibull analyses are reviewed for the three ferrite device geometries (0805, 1206, and 1806) and three material types (#43, #61, and #73). As in the case of the resistors and capacitors, the 2P Weibull data will be described, with the goal of presenting some quantitative trends as well as to provide the physical bases behind some of those trends. The 2P Weibull data reliability will be compared against the 10 ppm failure rate limit. As stipulated above, 3P Weibull analyses will still provide the accepted reliability predictions for the ferrite solder joints.

The 2P Weibull reliability data for the solder joint gap location are presented in Table14. Two parameters are cited for each of the manufacturing and storage conditions; they are the cycles to reach the 10 ppm failure rate (bright blue) and the failure rate at the end of the particular condition (bright red). These parameters, describe the reliability of only the individual segments. The same parameters of cycles to reach 10 ppm and the end-of-life failure rate were also provided for the four use conditions. In addition, two "cumulative effects" parameters were also computed for each of the use conditions; they were the "cumulative effect" cycles required to reach the 10 ppm failure rate (dark blue) in the use condition as well as the "cumulative effect" failure rate at the end of the use condition (dark red). As was stipulated in the description of the resistor and capacitor components, the "cumulative effect" values will serve as the accepted reliability metric for all of ferrite component devices.

The failure rates observed in the manufacturing cycles were predicted to exceed the 10 ppm limit for *only* the 0805 and 1806 ferrite devices made with material #43 and the latter also fabricated with the #61 material. Exceeding the failure limit in the manufacturing cycle would, therefore, preclude their being a "cumulative effect" cycles to a 10 ppm failure rate in the subsequent use conditions, because those cycles were already exhausted by the prior segment (i.e., the manufacturing segment). In all other cases of ferrite geometry and material composition, the failure rate did not exceed the 10 ppm limit, although the safety margin in some cases was quite limited. Finally, it was also observed that the storage environment had a negligible effect on the TMF life of the ferrite solder joints.

The failure rates of the ferrite solder joint gaps exceeded the 10 ppm limit for all sizes, all compositions, and under all use conditions. Moreover, the "cumulative effect" cycles required to reach the 10 ppm failure rate were well below the 5475 cycles comprising the 15 year service life, use conditions. An across-the-board comparison of reliability data between the 1206 ferrite parts versus the 1206 resistor and the 1210 capacitor indicated that TMF in the gaps of the ferrite solder joints (all material compositions) was generally *less than* the extent of damage that was predicted in the resistor and capacitor solder joint gaps. A similar conclusion was drawn when comparing the reliability of the 1806 ferrites versus the 1812 and 1825 capacitors. These two trends were the result of two attributes particular to the ferrite materials. First, the ferrite compositions generally had lower

elastic moduli as compared to the elastic modulus of the alumina which made up the resistor and capacitor components. The reduced modulus allowed the ferrite bodies to accommodate more of the thermal expansion mismatch strain rather than it be incorporated as TMF in the solder. Secondly, the ferrite materials had generally higher thermal expansion coefficients than alumina which permitted them to better match the higher thermal expansion coefficient of the printed circuit board laminate.

Three general observations were noted when comparing the reliability predictions as a function of ferrite size, material, and use condition: (1) In terms of relative reliability across the use conditions, the 1206 geometry faired the best, followed by the 0805 geometry. The 1806 ferrite configuration showed the lowest reliability, which was due to it being the longest part. Although being shortest part, the 0805 ferrite solder joint gap was less reliable than the longer 1206 geometry because the former used a smaller pad width (0.040 in.) as compared to the pad width for the1206 geometry (0.05 in.). The smaller pad width reduced the area over which the crack would be required to propagate to failure, thereby shortening the joint TMF lifetime.

(2) The #73 material offered the highest relative reliability per each part size and use condition, followed by the #61 material, and lastly the #43 composition. The higher thermal expansion coefficient of the #73 composition allowed this material to more closely match the thermal expansion coefficient of the printed circuit boards laminate, thereby reducing the amount of inelastic strain imparted into the solder. The #61 material had a better reliability performance than the #43 composition due primarily to a lower elastic modulus value. The reduced elastic modulus of the #61 composition allowed these components to more readily accommodate the thermal expansion mismatch displacement through its own elastic deformation rather than the mismatch displacement being relieved through inelastic deformation in the solder.

(3) A reliability trend was not determinable between *all* four use conditions (for the solder joint gap location). The only consistent behaviors were that the "B" use condition always provided the highest reliability and that the "A" use condition had the lowest reliability performance. The "C" and "D" use conditions exchanged relative reliability "status," depending upon the specific ferrite size and material composition.

Global thermal expansion mismatch strain still dominated the TMF process in the solder joint gaps. However, the magnitude of that dominance varied considerably between ferrite geometries, materials, and the use condition. Global mismatch strain was least prevalent with the 1206 geometry; it was most dominant with the1806 ferrite size, exactly inverse to the reliability trend predicted for these device sizes per material and use condition. Likewise, across-the-board, the highest reliability which was exhibited by the #73 material also corresponded to the lowest degree of global thermal expansion mismatch strain in the solder interconnects. The #43 material composition, which was characterized by the lowest reliability predictions, exhibited the greatest percentage of solder damage arising from global effects.

The results of the 2P Weibull analysis performed for the fillet location of the ferrite solder joints are provided in Table 15. Failure rates within the manufacturing and storage segments were well below the 10 ppm criterion. An overview of the ("cumulative effect") reliability numbers for the use conditions reveal that the 10 ppm limit was exceeded in all cases with the exception of the 0805 and 1206 ferrite geometries, when the latter were made with the #73 composition, and they were subjected to the "D" use condition. In general,1806 geometry exhibited the lowest relative reliability; the 0805 and 1206 geometries showed very similar behaviors. As was the case with the gap calculations, the #73 material offered the highest relative reliability per each part geometry and condition, followed by the #61 material and lastly the #43 composition. From amongst the four use conditions, the highest reliability was realized with the "D" use condition. The "A" use condition caused the lowest relative reliability with the exception of the 1806 ferrite made with the #73 material. The complex interplay between part (fillet) geometry, material behavior, and temperature cycle precluded there being any consistent trends between the "B" and "C" use conditions.

Global thermal expansion mismatch had a significantly reduced role in the TMF deformation/damage of the fillet locations. The 0805 ferrites exhibited between 16% and 34% of TMF was attributed to global mismatch, with the lower limit being observed for the #73 material and the higher limit resting with the #43 material. Per ferrite size, the inelastic strain contribution from global thermal expansion mismatch was greatest with the 1806 geometry, ranging from 57% to 68% of the total TMF deformation/damage in the solder joints. The extent to which global thermal expansion mismatch contributed to TMF showed an inverse relationship to the predicted fillet reliability. However, this correlation was weak in the case of the fillet simply due to its reduced contribution to TMF deformation/damage.

The 3P Weibull analysis established the accepted reliability predictions for the ferrite solder joints. The analysis begins with the gap location; those data are shown in Table 16. The "cumulative effect" cycles-to-first failure (dark blue); and the "cumulative effect" failure rate at the end of life (dark red) provided the reliability metrics. The 200 manufacturing cycles and 3650 storage cycles were well below the number of cycles required to reach first failure in each case.

The following general observations were made of the reliability predictions for the gap location per each of the use conditions: (1) The1206 geometry out-performed the other two ferrite sizes. In all but one instance, the #43 composition and use condition "A", there were no failures predicted for solder in the 1206 solder joint gaps. The "next-best" performer was the 0805 geometry, followed by the 1806 ferrite size.

(2) The #73 material was provided the highest relative reliability per part size and use condition, followed by the #61 material and lastly the #43 composition.

(3) The best reliability was realized with the "B" condition; the worst reliability was predicted for the "A" condition. No consistent trends were identified between the "C" and "D" use conditions.

A summary of the reliability computations for the gap region of the ferrite solder joints will be made at this point. Both the 2P and 3P Weibull analyses showed similar trends. The 3P Weibull "cumulative effect," end-of-life failure rate for the gap region ranged from 0% to 99%. This wide range of behavior was caused by the synergistic effects of the three variables: ferrite size, material composition, and use-condition. The loss of integrity by solder in the gap constitutes primarily a decrease in mechanical strength and no loss in electrical function.

Next, the 3P Weibull reliability evaluations were performed on the fillet locations of the ferrite solder joints. The data are shown in Table 17. The number of cycles representing the manufacturing and storage segments were well below the number of cycles required to see a first failure for either case. Under all circumstances of ferrite geometry, ferrite material, and use conditions, the 3P Weibull distribution predicted a "cumulative effect" failure rate of 0% at the end of each of the use. In fact, first failures were predicted to occur between three and fifteen *use conditions*.

In summary, the 3P Weibull, "cumulative effect" end-of-life failure rates in the 0.001 in. thick solder joint gap were predicted to exceed the 10 ppm limit in some, but not all, of the cases represented by ferrite size, ferrite material composition, and use condition. At the solder joint fillet locations, the 3P Weibull analysis predicted 0% failure rates for all cases of ferrite geometry, material, and use condition. Therefore, the ferrite solder joints will maintain a reliable electrical functionality over the manufacturing, storage, and potential use conditions of the product. Some loss of mechanical strength can be expected in selected geometry-material-use cases due to TMF damage in the gap locations.

Reliability computations for accelerated testing conditions

Leadless chip resistors and capacitors

The SRS™ software was exercised in order to determine the propensity for TMF failures to occur in the resistor and capacitor solder joints undergoing accelerated aging tests. As noted earlier, the accelerated tests used temperature limits of 0°C and 100°C; hold times of 15 min at each of the two temperature limits; and ramp rates of 10°C/min between the temperature limits. These parameters result in a cycle frequency of 28.8 cycles/day. The duration of testing was established at 3 months (0.25 years). As in the previous studies, both the 2P and 2P Weibull calculations were performed as in the previous studies. However, the "official" reliability predictions were drawn from the 3P Weibull analyses; the 2P Weibull data were used as a lower limit reliability benchmark.

Shown in Table 18 are the 2P and 3P Weibull reliability predictions for the chip resistors and capacitors. Results pertaining to both the gap (0.001 in.) and fillet locations have also been listed together in the table. The reliability predictions were based upon a 50% failure rate by the end of the accelerated tests. The 2P Weibull data include the cycles required to reach a failure rate of 50% (blue) and the predicted failure rate at the end of the test program (0.25 years, or 2628 cycles). The 3P Weibull prediction were described by: the number of failure free cycles (green); the number of cycles required to reach a

failure rate of 50% (blue); and the failure rate at the end of life (red). The number of cycles to a 50% failure rate in the 3P Weibull analysis was calculated using equation (8). The value of F(N) was equal to 0.5. The value of α was taken as the 2P Weibull characteristic life (63% failure rate); $N_{o,i}$ was the number of cycles to first failure; and β was the 3P Weibull slope taken to be 2.2. The 3P Weibull failure rate at the end of life, F(N=2628) was also computed using equation (8). In this computation, the value of N was equal to the cycles at the end of life, 2628.

A comparison was made between the accelerated test, reliability predictions of the gap location in the resistor and capacitor solder joints versus similar predictions under the four use conditions. Specifically, this comparison was made by examining the cycles to 50% failure under accelerated testing and the "cumulative effect" cycles to first failure per each use condition. It was observed that the same relative trends observed in the use conditions were reproduced under the accelerated test conditions. Therefore, a relative ranking of the reliability of the solder joint gap location, which was based upon resistor or capacitor part size, was not sensitive to the details of the temperature cycle.

An end of life failure rate of 100% was predicted by the 3P Weibull analysis for the gap locations of all chip capacitors and two of the three resistors; the third resistor (0805) had a 98% failure rate. Therefore, it is expected that the solder in the gap regions of nearly all of the resistor and capacitor joints will have failed at the end of the accelerated test cycles. Although not impacting the electrical performance of the joints, failure of the gap location will certainly be distinguishable in the metallographic cross sections as well as appear as a reduction in the solder joint shear strength.

The 3P Weibull analyses of the fillet location of the resistor and capacitor solder joins were evaluated. As was the case with the gap location, a relative rank-order of reliabilities between the three resistors and three capacitors was unchanged from the predictions made under each of the four use conditions . The 3P Weibull analysis predicted a 0% end-of-life failure rate for the solder joint fillets of all chip resistors and capacitors. The number of cycles required for the failure rate to approach 50% was nearly an order of magnitude greater than the duration of the test program. Therefore, since TMF failure of the solder joint fillets was not predicted, the accelerated testing program would not be expected to produce an electrical failure amongst the current counting of resistor or capacitor interconnects.

(From the 2P Weibull data, an 83 ppm failure rate was predicted at the end of accelerated testing of the 1206 resistor. That is, one can expect to observe 83 failures if one million 1206 resistors were tested under these conditions.)

Shown in Table 19 are the accelerated testing reliability predictions for the ferrite solder joints. The data have been categorized according to ferrite geometry and material. First, the gap location data will be examined. The 3P Weibull analysis indicated that a nominal reliability loss can be expected to occur in the gap regions of the solder joints. Moreover, the accelerated nature of the testing has clearly magnified the sensitivity of the TMF degradation to ferrite geometry and material. For example, in the case of the 0805 ferrite

geometry, the 3P Weibull analysis predicts a 100% failure rate if the chip is fabricated from the #43 material; however, a 0% failure rate is anticipated if the #73 composition was used for the device. A similar "wide-range" in gap location reliability was also observed for the 1806 ferrite size. The reliability numbers were somewhat tighter for the 1206 ferrite size, ranging from a 29% failure rate predicted with the #43 material to 0% failures with the #73 material. Therefore, the relative reliability rankings, from best to worst, for the ferrite geometries and materials are as follows: [1206, 0805, 1806] and [#73, #61, #43], respectively. The same relative reliability ranks were observed, using either the "cumulative effect" cycles-to-first failure or the "cumulative effect" end-of-life failure rate, when a comparison was made between the accelerated test data and the four use conditions. Therefore, as was the case with the resistors and capacitors, the ranking of relative reliabilities between the ferrite sizes and materials, was not sensitive, per se, to the temperature cycle.

Next, the 3P Weibull reliability predictions for the solder joint fillets were examined. As was the case with the solder joint gap location, the same relative reliability performances were observed after accelerated testing as were predicted under each of the four use conditions. The 3P Weibull analyses predicted 0% failures in the ferrite solder joint fillets at the end of the accelerated testing program. In the worst case of the 1806 ferrite size and #43 composition, a two-to-three fold increase in test duration would be required in order to observe a 50% failure rate. In fact, the test cycles climb to a value that is nearly an order of magnitude greater than the proposed test length when considering either 0805 or 1206 ferrite geometries using the #73 material. Therefore, no electrical failures would be expected during the course of such testing.

A summary is made of the 3P Weibull predictions for TMF failure as a consequence of exposing the resistors, capacitors, and ferrite solder joints to the specified accelerated testing regime. Those test conditions were predicted to cause a 98% to100% failure rate in the gap locations of all resistor and capacitor interconnects. However, a 0% failure rate was predicted in the fillet locations after accelerated testing. The failure rates predicted for the gap location of the ferrite solder joints varied considerably as a function of the different component sizes and material compositions. However, 0% failure rates were predicted in the fillet regions of the ferrite solder joints for all geometries and materials. Therefore, although the accelerated test conditions would result in a loss of mechanical strength to the solder joints, more so in the case of the resistors and capacitors than in the case of the ferrites. However, no electrical failures were predicted for any of the device solder joints.

Role of the Sandia TMF computational model.
The above analysis predicted that the chip resistor, capacitor, and ferrite solder joints would not experience an electrical failure as a consequence of either accelerated testing or manufacturing-storage-use environments. The (successful) long-term reliability predicted by the SRS™ analysis was a result, in large-part, of the limited amount of TMF that was predicted to occur in the fillet location of the solder joints. However, it must be fully appreciate that the determination of an effective gap thickness to represent the fillet location in the SRS™ computation, was based largely upon qualitative observations and

a degree of engineering judgment. Such a critical parameter for the SRS™ reliability prediction should be based upon a more thorough analysis of TMF behavior taking place *in the fillet*. Therefore, the Sandia computational model should be used to investigate TMF behavior in the fillets of these solder joints. A functional expression that can be used to determine (albeit, estimate …) an effective gap width would be derived from that analysis. That effective gap value would then be used in the SRS™ software to more accurately determine the TMF reliability of solder joint fillet.

Conclusions

1. The SRS™ software provided reliability predictions of the thermal mechanical fatigue (TMF) failure of solder joints for three sizes of chip resistors, three sizes of chip capacitors, as well as three sizes and three material compositions of ferrite chip inductors. All devices were assumed to have been assembled on a "high-end," FR-4 laminate printed wiring board. Four "use" conditions and one accelerated testing condition were assessed. The end-of-life failure rate maximum was 10 ppm for the use conditions and 50% after accelerated testing. The 3P Weibull predictions determined the accepted reliability numbers. The analyses were performed for both the gap location (0.001 in. thick) and fillet location of the leadless solder joints. Failure of solder in the gap would result in a reduced joint strength, but no loss of electrical functionality. Fatigue failure of solder in the fillet, which would occur subsequent to failure of solder in the gap, would result in a complete loss of mechanical integrity and electrical continuity.

2. The "cumulative effect" end-of-life failure rates for the solder joint gaps of the resistors and capacitors will exceed the10 ppm limit in nearly every case of component size and use condition. At the solder joint fillet locations, no failures were predicted for all cases of component size and use condition. Therefore, the chip resistors and capacitors would provide reliable electrical functionality over any of the product use cycles. The reduced joint strength must accommodate subsequent transportation, flight and target sequence loads.

3. The "cumulative effect" end-of-life failure rates for the solder joint gaps of the ferrite inductors would exceed the 10 ppm limit in some, but not all, of the cases represented by component size, ferrite material, and use condition. At the solder joint fillet locations, a 0% failure rate was predicted for all cases of ferrite size, material, and use condition. Therefore, the ferrite components would provide reliable electrical functionality over the entire product lifetime. The lower joint strength due to fatigue failure in the gap must accommodate transportation, flight and target sequence loads.

4. The accelerated test conditions were predicted to cause a decrease in mechanical strength in the resistor, capacitor, and ferrite inductor solder joints, more so in the case of the resistors and capacitors and to a lesser degree, for the ferrite components. However, the absence of predicted TMF failure in the solder joint fillets implies that no catastrophic loss of mechanical integrity or electrical performance were predicted for any of the devices.

References

[1] R. Prasad: [limit chip sizes to <2512 for glass fiber boards].
[2] Raytheon source: [limit the maximum size of ceramic packages to <0.375 in.].
[3] B.F. Goodrich: [limit maximum length of ceramic package to <0.200 in.].
[4] "Guidelines for Accelerated Reliability Testing of Surface Mount Solder Attachments," IPC-SM-785 (The Institute for Interconnecting and Packaging Electronic Circuits; Northbrook, IL; 1992), p. 20.
[5] "Qualification and Performance Test Methods for Surface Mount Solder Attachments," IPC-9701 (The Institute for Interconnecting and Packaging Electronic Circuits; Northbrook, IL; 1998).
[6] SRS™1.1, or Solder Reliability Solutions™ Version 1.1, is a product of Electronics Packaging Solutions International, Inc., Montclair, NJ.
[7] J.P. Cleche, "Solder Reliability Solutions – A PC-Based Design-for-Reliability Tool," *Proc. Surface Mount International Conference* (SMTA, San Jose, CA; September 8-12, 1996), pp. 136-151.
[8] J.P. Cleche, et al, "Surface Mount Assembly Failure Statistics and Failure Free Time," *Proc. 44th ECTC* (IEEE, Washington, DC, May 1-4, 1994), pp. 487-497.
[9] "Surface Mount Land Patterns (Configurations and Design Rules," (The Institute for Interconnecting and Packaging Electronic Circuits; Northbrook, IL; 1987), pp. 5-7.
[10] "Ferrite Pad Design," K. Olsberg (memorandum to P. Vianco and S. Burchett dtd. August 22, 2000, Sandia National Laboratories, Albuquerque, NM).
[11] W. Kingery, H. Bown, and D. Uhlmann, *Introduction to Ceramics* (J. Wiley and Sons; New York, NY; 1976), pp. 594-595, 777.
[12] C. Chirigos, "Information Retrieval – Thermal Expansion," memorandum to Distribution dtd. November 20, 1985 (Sandia National Laboratories, Albuquerque, NM).
[13] *Electronic Materials and Processes Handbook* ed. by C. Harper and R. Sampson (McGraw-Hill; New York, NY; 1994), pp. 5.57-5.65.
[14] G. Carter, *Principles of Physical and Chemical Metallurgy* (ASM, Inter.; Materials Park, OH; 1979), p. 103.

Distribution:

1	MS0874	J.N. Sweet, 1745
1	MS0874	R.W. Wavrik, 1745
1	MS1435	A. K. Hays, 1800
1	MS0885	M.J. Cieslak, 1801
1	MS1434	D. B. Dimos, 1802
1	MS1411	H.E. Fang, 1834
1	MS0367	R. J. Salzbrenner, 1835
1	MS1411	Jerome Rejent, 1835
4	MS1411	Paul Vianco, 1835
1	MS0367	F. Michael Hosking, 1833
1	MS0367	J. J. Stephens, 1833
1	MS0847	M.K. Neilsen, 9123
1	MS0847	A.F. Fossum, 9123
2	MS0847	S.N. Burchett, 9126
1	MS9018	Central Technical Files, 8945-1
2	MS0899	Technical Library, 9616
1	MS0612	Review & Approval Desk, 9612

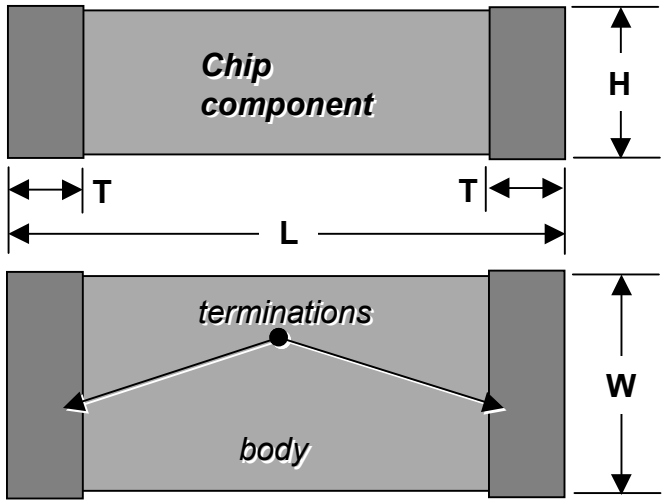

Fig. 1 Schematic diagram showing the dimension notation of the chip components.

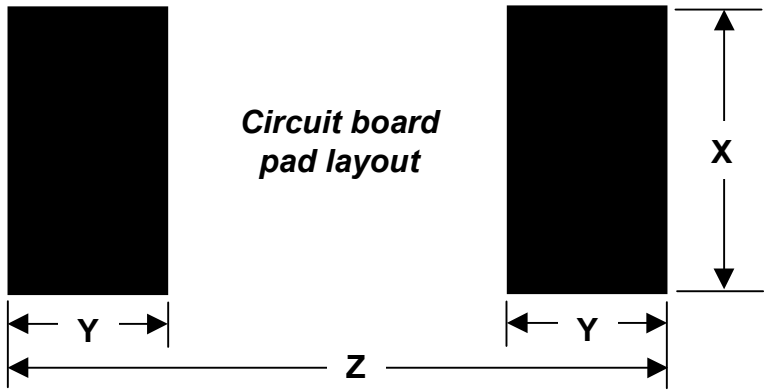

Fig. 2 Schematic diagram showing the circuit board bond land pattern configuration..

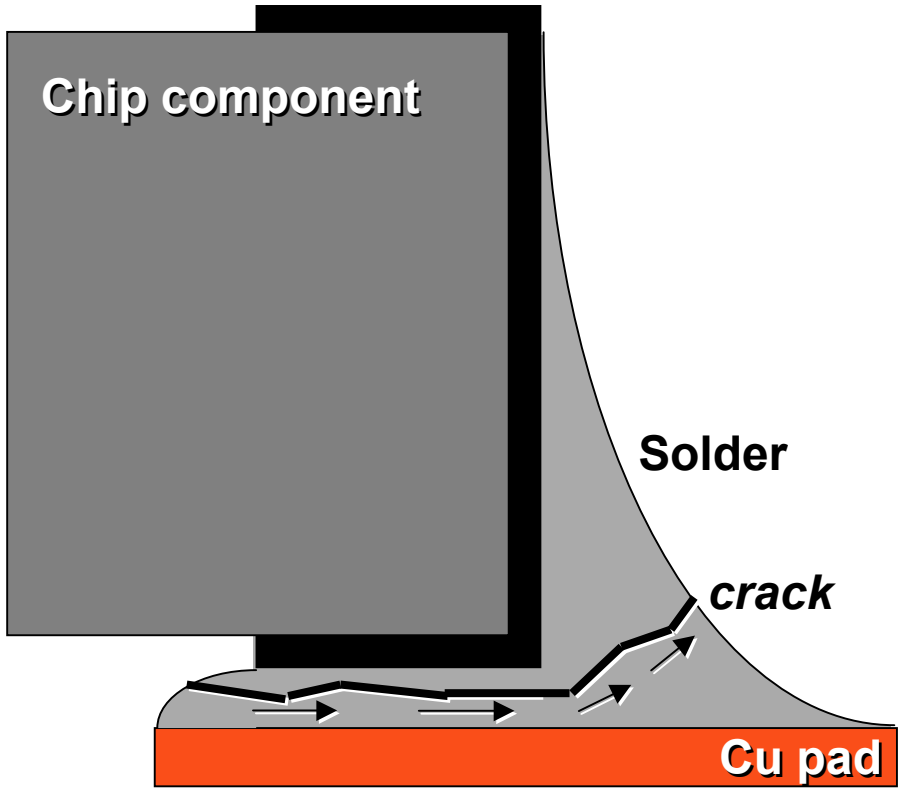

Fig. 3a Diagram showing crack propagation through the solder joint of a chip component.

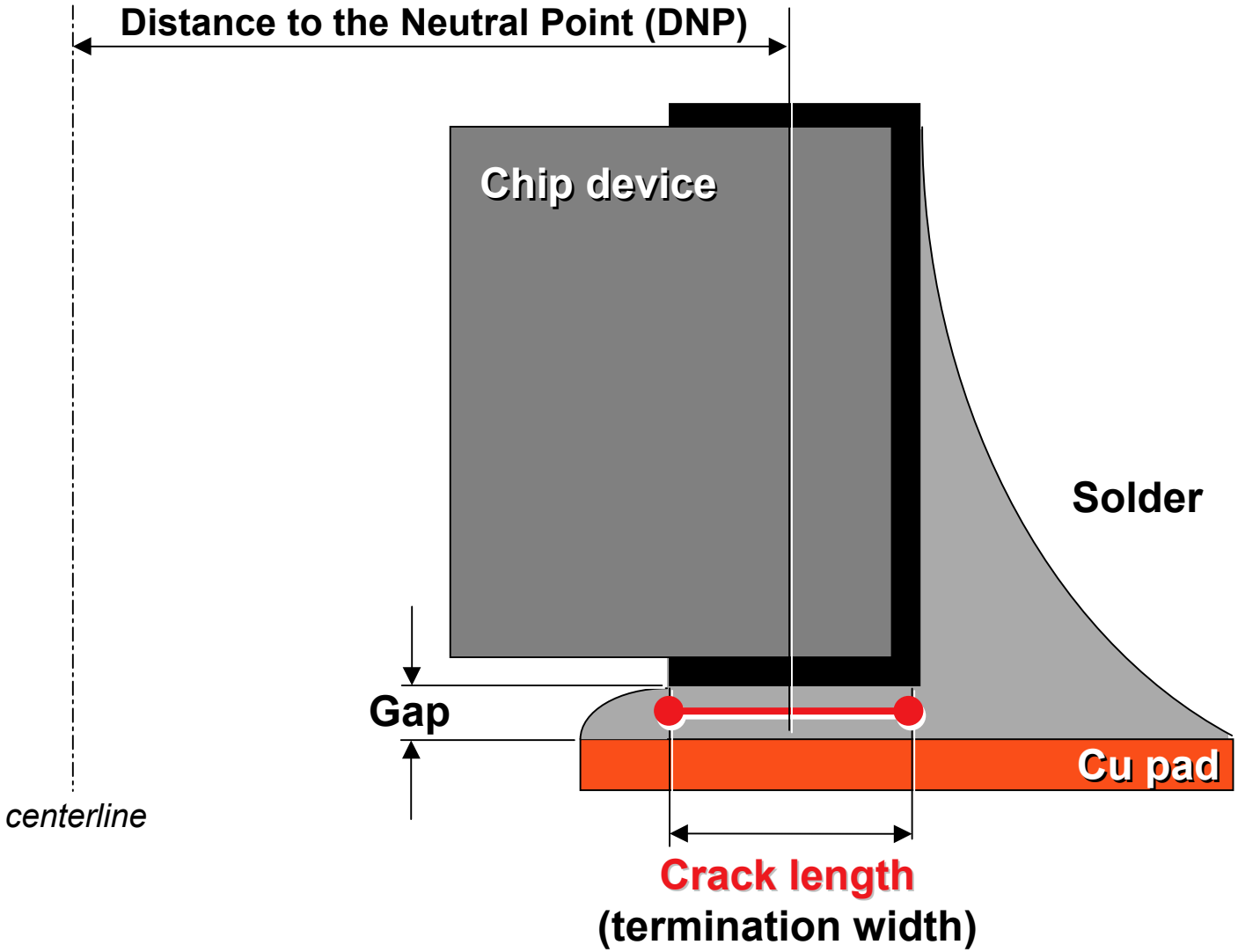

Fig. 3b Geometry for predicting thermal mechanical fatigue (TMF) in the gap location of the chip component solder joints.

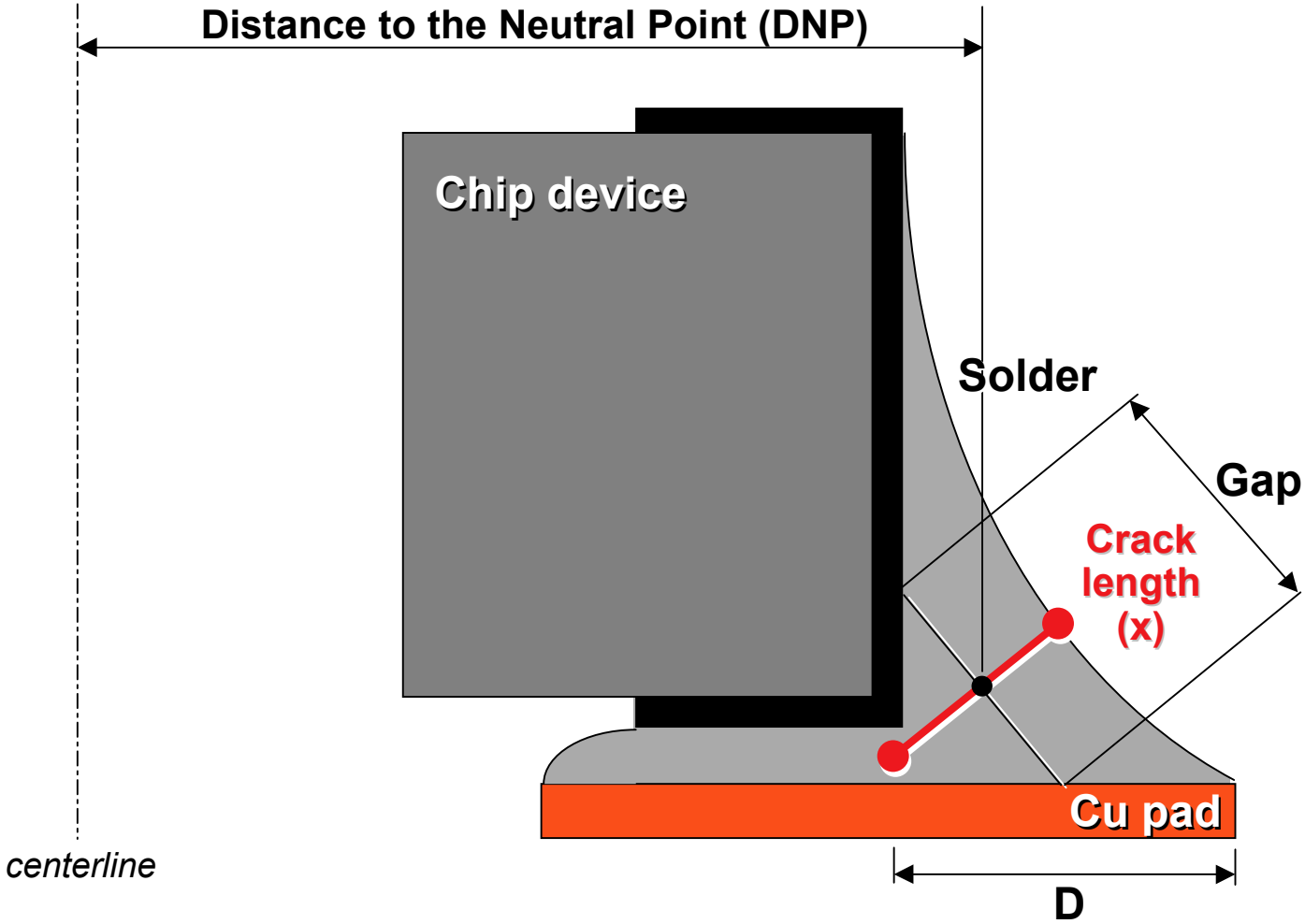

Fig. 3c Geometry for predicting thermal mechanical fatigue (TMF) in the fillet location of the chip component solder joints.

Table 1
Temperature Cycles for the Life Cycle Manufacturing and Storage Segments

Segment	Lower Temperture Limit (°C)	Upper Temperature Limit (°C)	ΔT (°C)	Number of Cycles	Dwell Time At the Temperature Limits (min)
Manufacturing	20	80	60	200	60
Storage	17	23	6	3650	720

Table 2
Temperature Cycles for the Life Cycle "Use" Conditions

Use Condition	Lower Temperture Limit (°C)	Upper Temperature Limit (°C)	ΔT (°C)	Number of Cycles	Dwell Time At the Temperature Limits (min)
"A"	20	55	35	5475	720
"B"	-10	20	30	5475	720
"C"	10	40	30	5475	720
"D"	40	70	30	5475	720

Table 3
Dimensions of the Resistors, Capacitors, and Ferrite Components

Component	Length L (in.)	Width W (in.)	Height H (in.)	Termination Width T (in.)
1206 Resistor	0.120	0.060	0.022	0.022
2010 Resistor	0.200	0.100	0.047	0.022
2512 Resistor	0.250	0.120	0.047	0.022
1210 Capacitor	0.120	0.100	0.067	0.022
1812 Capacitor	0.180	0.120	0.067	0.022
1825 Capacitor	0.180	0.250	0.067	0.022
0805 Ferrite	0.080	0.050	0.039	0.020
1206 Ferrite	0.128	0.064	0.044	0.028
1806 Ferrite	0.180	0.064	0.064	0.028

Table 4a
Thermal Expansion Coefficients Over Temperature Steps Between 50°C and 200°C for the Cylindrical ("Kit") and Rectangular Samples

Temperature Interval (°C)	Thermal Expansion Coefficient ($x10^{-6}$ $°C^{-1}$)					
	#43 Material		#61 Material		#73 Material	
	Cyl.	Rect.	Cyl.	Rect.	Cyl.	Rect.
-50, -25	4.53	3.97	3.82	6.15	5.21	5.42
-25, 0	6.36	5.92	6.75	5.66	8.69	8.63
0, 25	5.59	7.34	6.34	6.40	7.97	6.98
25, 50	8.18	6.67	7.19	7.37	11.0	10.2
50, 75	8.25	7.69	9.60	7.58	11.4	11.0
75, 100	8.23	7.38	9.54	8.25	12.4	13.1
100, 125	9.17	8.23	8.50	8.97	13.6	14.1
125, 150	8.69	9.22	9.86	8.79	14.0	14.8
150, 175	8.75	9.27	10.4	9.10	14.2	15.1
175, 200	8.96	9.01	8.58	9.16	11.8	15.5

Table 4b
Thermal Expansion Coefficients Over Temperature Steps Between 50°C and 200°C for #65 Cylindrical (Kit) and Chip Ferrite Samples

Temperature Interval (°C)	Thermal Expansion Coefficient ($x10^{-6}$ $°C^{-1}$)			
	#65 Material Cyl.	BUM41P0312.	257T612	257X111
-50, -25	0.901	2.13	4.76	6.13
-25, 0	3.11	4.76	7.21	6.63
0, 25	1.89	9.16	5.47	7.42
25, 50	3.85	7.45	7.79	7.04
50, 75	5.40	8.79	8.95	7.35
75, 100	8.17	8.34	6.57	5.90
100, 125	7.39	7.96	7.46	8.89
125, 150	8.58	8.10	-----	6.87
150, 175	9.19	7.21	-----	5.78
175, 200	9.06	7.48	-----	6.96

Table 5
Thermal Expansion Coefficients for the Ferrite Cylinder ("Kit") Materials Over the Manufacturing, Storage, and "Use" Conditions

Use Condition	Thermal Expansion Coefficient ($x10^{-6}$ $°C^{-1}$)		
	#43 Material	#61 Material	#73 Material
Manufacturing	8.22	8.22	11.2
Storage	5.64	7.01	8.61
"A"	8.18	7.19	11.0
"B"	6.77	6.55	8.65
"C"	6.56	6.76	9.50
"D"	8.25	7.95	11.4

Table 6
Density Values for the Ferrite Cylinder ("Kit") and Rectangular Materials

Specimen	Density (g/cm^3)					
	#43 Material		#61 Material		#73 Material	
	Cyl.	Rect.	Cyl.	Rect.	Cyl.	Rect.
#1	4.78	5.05	4.96	5.05	4.65	4.61
#2	4.95	5.07	4.75	5.04	4.65	4.61
Average	4.87	5.06	4.86	5.05	4.65	4.61

Table 7
Young's (Elastic) Modulus for the Ferrite Rectangular Materials Over the Manufacturing, Storage, and "Use" Conditions

Use Condition	Youmg's (Elastic) Modulus ($x10^6$ psi)		
	#43 Material	#61 Material	#73 Material
Manufacturing	23.4	14.1	19.3
Storage	23.5	14.1	19.5
"A"	23.4	14.1	19.4
"B"	23.4	14.1	19.5
"C"	23.4	14.1	19.5
"D"	23.4	14.0	19.3

Table 8
Dimensions of the PWB Land Patterns for the Resistors, Capacitors, and Ferrite Chip Components

Component	End-to-End Distance Z (in.)	Pad Width X (in.)	Pad Length Y (in.)
1206 Resistor	0.200	0.063	0.063
2010 Resistor	0.360	0.100*	0.113
2512 Resistor	0.410	0.120*	0.109
1210 Capacitor	0.213	0.102	0.070
1812 Capacitor	0.268	0.126	0.070
1825 Capacitor	0.268	0.260	0.070
0805 Ferrite	0.140	0.040	0.055
1206 Ferrite	0.185	0.050	0.065
1806 Ferrite	0.235	0.050	0.065

* Assuming that the resistors held to the maximum width, the design rule in IPC-SM-782 would permit a land width less than the width of the component. Therefore, the nominal width was set equal to that of the chip device.

Table 9
Effective Parameters for Predicting TMF in the Fillet Location of the Resistors, Capacitors, and Ferrite Chip Components

Component	Solder Joint Gap (in.)	Crack Area (in^2.)	Distance to the Neutral Point (DNP) (in.)
1206 Resistor	0.028	0.0017	0.070
2010 Resistor	0.057	0.0057	0.120
2512 Resistor	0.057	0.0068	0.145
1210 Capacitor	0.033	0.0033	0.072
1812 Capacitor	0.031	0.0037	0.101
1825 Capacitor	0.031	0.0078	0.101
0805 Ferrite	0.021	0.00084	0.0475
1206 Ferrite	0.021	0.00105	0.0713
1806 Ferrite	0.020	0.00100	0.0970

Table 10
Two-Parameter (2P) Weibull Predictions for the Resistors and Capacitors - Gap (0.001 in.) Location
Cycles to the Failure Rate (F) of 10 ppm
(Failure Rate at the End of Life, F(n_i), "Cumulative Effect")

Component	Manufacturing [20°C … 80°C] Cyles to F = 10 ppm (n_i = 200 cycles)	Storage [17°C … 23°C] Cyles to F = 10 ppm (n_i = 3650 cycles)	Use Condition "B" [-10°C … 20°C] Cycles to F = 10 ppm (n_i = 5475 cycles)	Use Condition "C" [10°C … 40°C] Cycles to F = 10 ppm (n_i = 5475 cycles)	Use Condition "A" [20°C … 55°C] Cycles to F = 10 ppm (n_i = 5475 cycles)	Use Condition "D" [40°C … 70°C] Cycles to F = 10 ppm (n_i =5475 cycles)
1206 Resistor	146	83130	1214 (1.2%)	546 (16%)	304 (76%)	365 (52%)
2010 Resistor	45	14280	219 (99%)	161 (100%)	109 (100%)	143 (100%)
2512 Resistor	41	15550	213 (99%)	150 (100%)	100 (100%)	130 (100%)
1210 Capacitor	63	7959	227 (100%)	204 (100%)	150 (100%)	204 (99%)
1812 Capacitor	44	7057	172 (100%)	148 (100%)	106 (100%)	143 (100%)
1825 Capacitor	94	15550	373 (57%)	319 (77%)	228 (99%)	306 (82%)

Table 11
Two-Parameter (2P) Weibull Predictions for the Resistors and Capacitors - Fillet Location
Cycles to the Failure Rate of 10 ppm
(Failure Rate at the End of Life, "Cumulative Effect")

Component	Manufacturing [20°C … 80°C] Cyles to F = 10 ppm (n_i = 200 cycles)	Storage [17°C … 23°C] Cyles to F = 10 ppm (n_i = 3650 cycles)	Use Condition "B" [-10°C … 20°C] Cycles to F = 10 ppm (n_i = 5475 cycles)	Use Condition "C" [10°C … 40°C] Cycles to F = 10 ppm (n_i = 5475 cycles)	Use Condition "A" [20°C … 55°C] Cycles to F = 10 ppm (n_i = 5475 cycles)	Use Condition "D" [40°C … 70°C] Cycles to F = 10 ppm (n_i =5475 cycles)
1206 Resistor	2631	193800	7399 (5.0 ppm)	7085 (6.0 ppm)	5328 (16 ppm)	7285 (5.0 ppm)
2010 Resistor	8336	582900	22740 (0.05 ppm)	22130 (0.06 ppm)	16980 (0.2 ppm)	23490 (0.05 ppm)
2512 Resistor	9828	699400	27270 (0.03 ppm)	26290 (0.03 ppm)	19890 (0.08 ppm)	27280 (0.03 ppm)
1210 Capacitor	3046	191800	7675 (4.1 ppm)	7833 (3.8 ppm)	6292 (8.3 ppm)	8908 (2.4 ppm)
1812 Capacitor	2572	174700	6752 (7.0 ppm)	6770 (7.0 ppm)	5386 (16 ppm)	7568 (5.0 ppm)
1825 Capacitor	5437	372100	14320 (0.3 ppm)	14350 (0.3 ppm)	11400 (0.8 ppm)	16010 (0.2 ppm)

Table 12

Three-Parameter (3P) Weibull Predictions for the Resistors and Capacitors - Gap (0.001 in.) Location

Cycles to First Failure ("Cumulative Effect" Failure Free Time, yrs.)

Cycles to First Failure, "Cumulative Effect" (Failure Rate at End of Life, "Cumulative Effect")

Component	Manufacturing [20°C … 80°C] Cyles to First Failure (n_i = 200 cycles)	Storage [17°C … 23°C] Cyles to First Failure (n_i = 3650 cycles)	Use Condition "B" [-10°C … 20°C] Cycles to First Failure (n_i = 5475 cycles)		Use Condition "C" [10°C … 40°C] Cycles to First Failure (n_i = 5475 cycles)		Use Condition "A" [20°C … 55°C] Cycles to First Failure (n_i = 5475 cycles)		Use Condition "D" [40°C … 70°C] Cycles to First Failure (n_i =5475 cycles)	
1206 Resistor	1542	879000	12840 (30)	10950 (0%)	5770 (14)	5110 (15%)	3217 (7.6)	2774 (65%)	3864 (9.2)	3358 (34%)
2010 Resistor	472	151000	2314 (3.5)	1277 (94%)	1705 (2.6)	949 (100%)	1155 (1.7)	620 (100%)	1509 (2.3)	839 (100%)
2512 Resistor	433	164480	2256 (3.2)	1168 (95%)	1588 (2.2)	803 (100%)	1059 (1.5)	547 (100%)	1274 (1.9)	693 (100%)
1210 Capacitor	671	84160	2401 (4.3)	1596 (94%)	2160 (3.9)	1423 (98%)	1589 (2.9)	1058 (100%)	2158 (3.9)	1423 (98%)
1812 Capacitor	462	74620	1823 (2.6)	948 (100%)	1568 (2.2)	803 (100%)	1124 (1.6)	584 (100%)	1511 (2.1)	766 (100%)
1825 Capacitor	991	163900	3940 (8.4)	3066 (35%)	3370 (7.2)	2628 (58%)	2413 (5.1)	1861 (95%)	3236 (6.9)	2518 (64%)

Table 13
Three-Parameter (3P) Weibull Predictions for the Resistors and Capacitors - Fillet Location

	Cycles to First Failure ("Cumulative Effect" Failure Free Time, yrs.)		Cycles to First Failure, "Cumulative Effect" (Failure Rate at End of Life, "Cumulative Effect")							
Component	Manufacturing [20°C … 80°C] Cyles to First Failure (n_i = 200 cycles)	Storage [17°C … 23°C] Cyles to First Failure (n_i = 3650 cycles)	Use Condition "B" [-10°C … 20°C] Cycles to First Failure (n_i = 5475 cycles)		Use Condition "C" [10°C … 40°C] Cycles to First Failure (n_i = 5475 cycles)		Use Condition "A" [20°C … 55°C] Cycles to First Failure (n_i = 5475 cycles)		Use Condition "D" [40°C … 70°C] Cycles to First Failure (n_i =5475 cycles)	
1206 Resistor	27820	2049000	78230 (212)	77379 (0%)	74920 (203)	74095 (0%)	56340 (153)	55845 (0%)	77030 (209)	76285 (0%)
2010 Resistor	86160	6200000	240000 (656)	239440 (0%)	230000 (639)	233235 (0%)	179500 (490)	178850 (0%)	250000 (678)	247470 (0%)
2512 Resistor	103900	7400000	288300 (788)	287620 (0%)	277900 (759)	277035 (0%)	210400 (574)	209510 (0%)	288500 (788)	287620 (0%)
1210 Capacitor	32210	2030000	81150 (220)	80300 (0%)	82820 (225)	82125 (0%)	66530 (181)	66065 (0%)	94190 (256)	93440 (0%)
1812 Capacitor	27200	1800000	71390 (194)	70810 (0%)	71590 (194)	70810 (0%)	56940 (154)	56210 (0%)	80030 (217)	79205 (0%)
1825 Capacitor	57490	3900000	151400 (413)	150745 (0%)	151700 (414)	151110 (0%)	120000 (328)	119720 (0%)	169300 (462)	168630 (0%)

Table 14

Two-Parameter (2P) Weibull Predictions for the Ferrite Components - Gap (0.001 in.) Location

	Cycles to the Failure Rate of 10 ppm (Failure Rate at the End of Life)		Cycles to the Failure Rate of 10 ppm, "Cumulative Effect" (Failure Rate at the End of Life, "Cumulative Effect")									
Component	Manufacturing [20°C … 80°C] Cyles to F = 10 ppm (n_i = 200 cycles)	Storage [17°C … 23°C] Cyles to F = 10 ppm (n_i = 3650 cycles)	Use Condition "B" [-10°C … 20°C] Cycles to F = 10 ppm (n_i = 5475 cycles)		Use Condition "C" [10°C … 40°C] Cycles to F = 10 ppm (n_i = 5475 cycles)		Use Condition "A" [20°C … 55°C] Cycles to F = 10 ppm (n_i = 5475 cycles)		Use Condition "D" [40°C … 70°C] Cycles to F = 10 ppm (n_i =5475 cycles)	
0805 #43 Material	143 (38 ppm)	30710 (2 ppb)	589 (7.2%)	- - - - (13%)	358 (42%)	- - - - (55%)	320 (58%)	- - - - (70%)	411 (27%)	- - - - (38%)
0805 #61 Material	238 (5 ppm)	80004 (0.04 ppb)	1173 (0.5%)	131 (1.0%)	613 (6.2%)	69 (8.9%)	388 (35%)	44 (42%)	551 (9.3%)	63 (13%)
0805 #73 Material	417 (0.5 ppm)	81380 (0.04 ppb)	1285 (0.03%)	610 (0.05%)	858 (1.6%)	408 (2.2%)	773 (2.5%)	367 (3.3%)	1046 (0.7%)	497 (1.0%)
1206 #43 Material	252 (4 ppm)	80070 (0.04 ppb)	1482 (0.19%)	232 (0.43%)	621 (5.9%)	98 (8.4%)	492 (14%)	78 (18%)	583 (7.5%)	92 (10%)
1206 #61 Material	545 (0.2 ppm)	164400 (0.002 ppb)	3247 (81 ppm)	1978 (0.01%)	1369 (0.25%)	835 (0.36%)	682 (4.1%)	416 (4.9%)	869 (1.6%)	530 (2.0%)
1206 #73 Material	954 (19 ppb)	173800 (0.002 ppb)	3454 (63 ppm)	2655 (0.01%)	1845 (0.08%)	1419 (0.11%)	1409 (0.23%)	1083 (0.29%)	1683 (0.11%)	1294 (0.14%)

Table 14 *(con't)*

Two-Parameter (2P) Weibull Predictions for the Ferrite Components - Gap (0.001 in.) Location

	Cycles to the Failure Rate of 10 ppm (Failure Rate at the End of Life)		Cycles to the Failure Rate of 10 ppm, "Cumulative Effect" (Failure Rate at the End of Life, "Cumulative Effect")							
Component	Manufacturing [20°C … 80°C] Cyles to F = 10 ppm (n_i = 200 cycles)	Storage [17°C … 23°C] Cyles to F = 10 ppm (n_i = 3650 cycles)	Use Condition "B" [-10°C … 20°C] Cycles to F = 10 ppm (n_i = 5475 cycles)		Use Condition "C" [10°C … 40°C] Cycles to F = 10 ppm (n_i = 5475 cycles)		Use Condition "A" [20°C … 55°C] Cycles to F = 10 ppm (n_i = 5475 cycles)		Use Condition "D" [40°C … 70°C] Cycles to F = 10 ppm (n_i =5475 cycles)	
1806 #43 Material	88 (269 ppm)	28180 (3 ppb)	426 (24%)	- - - - (42%)	224 (97%)	- - - - (99%)	194 (100%)	- - - - (100%)	244 (92%)	- - - - (98%)
1806 #61 Material	162 (23 ppm)	91980 (0.02 ppb)	989 (0.9%)	- - - - (2.1%)	421 (25%)	- - - - (34%)	245 (92%)	- - - - (96%)	339 (49%)	- - - - (13%)
1806 #73 Material	289 (2.3 ppm)	89730 (0.03 ppb)	1042 (0.08%)	277 (0.13%)	585 (7.4%)	155 (10%)	504 (13%)	134 (17%)	658 (4.7%)	175 (6.5%)

Table 15
Two-Parameter (2P) Weibull Predictions for the Ferrite Components - Fillet Location

Cycles to the Failure Rate of 10 ppm (Failure Rate at the End of Life, ppm) | **Cycles to the Failure Rate of 10 ppm, "Cumulative Effect" (Failure Rate at the End of Life, ppm, "Cumulative Effect")**

Component	Manufacturing [20°C … 80°C] Cyles to F = 10 ppm (n_i = 200 cycles)	Storage [17°C … 23°C] Cyles to F = 10 ppm (n_i = 3650 cycles)	Use Condition "B" [-10°C … 20°C] Cycles to F = 10 ppm (n_i = 5475 cycles)		Use Condition "C" [10°C … 40°C] Cycles to F = 10 ppm (n_i = 5475 cycles)		Use Condition "A" [20°C … 55°C] Cycles to F = 10 ppm (n_i = 5475 cycles)		Use Condition "D" [40°C … 70°C] Cycles to F = 10 ppm (n_i =5475 cycles)	
0805 #43 Material	1353 (0.005)	84900 (0.00003)	3284 (77)	2657 (119)	3016 (109)	2440 (163)	2857 (135)	2312 (197)	4002 (35)	3228 (59)
0805 #61 Material	1684 (0.002)	138400 (0.000005)	4221 (28)	3607 (43)	3923 (38)	3353 (56)	3096 (98)	2646 (134)	4697 (19)	4014 (30)
0805 #73 Material	2316 (0.0006)	146200 (0.000004)	4704 (18)	4180 (26)	4900 (16)	4354 (23)	4688 (19)	4166 (27)	6925 (4)	6153 (7)
1206 #43 Material	1302 (0.006)	90410 (0.00004)	3306 (75)	2664 (117)	2932 (122)	2363 (181)	2789 (149)	2248 (217)	3871 (40)	3120 (67)
1206 #61 Material	1685 (0.002)	158000 (0.000003)	4495 (22)	3857 (34)	3976 (36)	3412 (53)	3078 (100)	2641 (136)	4655 (19)	3994 (30)
1206 #73 Material	2405 (0.0005)	166300 (0.000002)	4995 (14)	4470 (20)	5058 (14)	4526 (20)	4875 (16)	4362 (23)	7163 (3)	6409 (5)

Table 15 *(con't)*

Two-Parameter (2P) Weibull Predictions for the Ferrite Components - Fillet Location

	Cycles to the Failure Rate of 10 ppm (Failure Rate at the End of Life, ppm)		Cycles to the Failure Rate of 10 ppm, "Cumulative Effect" (Failure Rate at the End of Life, ppm, "Cumulative Effect")							
Component	Manufacturing [20°C … 80°C] Cyles to F = 10 ppm (n_i = 200 cycles)	Storage [17°C … 23°C] Cyles to F = 10 ppm (n_i = 3650 cycles)	Use Condition "B" [-10°C … 20°C] Cycles to F = 10 ppm (n_i = 5475 cycles)		Use Condition "C" [10°C … 40°C] Cycles to F = 10 ppm (n_i = 5475 cycles)		Use Condition "A" [20°C … 55°C] Cycles to F = 10 ppm (n_i = 5475 cycles)		Use Condition "D" [40°C … 70°C] Cycles to F = 10 ppm (n_i =5475 cycles)	
1806 #43 Material	712 (0.062)	38780 (0.0008)	1645 (1000)	1028 (1532)	1538 (2000)	961 (2984)	1528 (2000)	955 (2976)	2141 (428)	1337 (740)
1806 #61 Material	875 (0.027)	83850 (0.000036)	2191 (391)	1594 (591)	2047 (513)	1489 (756)	1634 (1300)	1189 (1780)	2525 (222)	1837 (356)
1806 #73 Material	1343 (0.0006)	83920 (0.000004)	2530 (220)	2044 (309)	2737 (161)	2211 (232)	2796 (147)	2258 (214)	4196 (29)	3388 (50)

Table 16
Three-Parameter (3P) Weibull Predictions for the Ferrite Components - Gap (0.001 in.) Location

Cycles to First Failure ("Cumulative Effect" Failure Free Time, yrs.) | **Cycles to First Failure, "Cumulative Effect" (Failure Rate at End of Life, "Cumulative Effect")**

Component	Manufacturing [20°C … 80°C] Cyles to F = 10 ppm (n_i = 200 cycles)	Storage [17°C … 23°C] Cyles to F = 10 ppm (n_i = 3650 cycles)	Use Condition "B" [-10°C … 20°C] Cycles to F = 10 ppm (n_i = 5475 cycles)		Use Condition "C" [10°C … 40°C] Cycles to F = 10 ppm (n_i = 5475 cycles)		Use Condition "A" [20°C … 55°C] Cycles to F = 10 ppm (n_i = 5475 cycles)		Use Condition "D" [40°C … 70°C] Cycles to F = 10 ppm (n_i =5475 cycles)	
0805 #43 Material	1509	324800	6228 (14.6)	5331 (0.04%)	3787 (8.9)	3242 (38%)	3381 (7.9)	2894 (57%)	4345 (10.2)	3719 (19%)
0805 #61 Material	2519	846300	12400 (31)	11359 (0%)	6486 (16.3)	5942 (0%)	4102 (10.3)	3758 (23%)	5827 (14.6)	5338 (0.05%)
0805 #73 Material	4408	860500	13590 (35)	12914 (0%)	9068 (23.6)	8617 (0%)	8174 (21.3)	7768 (0%)	11060 (28.8)	10510 (0%)
1206 #43 Material	2659	846700	15670 (40)	14420 (0%)	6568 (16.6)	6045 (0%)	5201 (13.1)	4787 (2.1%)	6168 (15.6)	5677 (0%)
1206 #61 Material	5757	1700000	34330 (90)	33061 (0%)	14480 (38)	13946 (0%)	7209 (19)	6943 (0%)	9183 (24)	8844 (0%)
1206 #73 Material	10090	1800000	36520 (98)	35721 (0%)	19510 (52)	19084 (0%)	14900 (40)	14574 (0%)	17790 (47)	17401 (0%)

Table 16 *(con't)*

Three-Parameter (3P) Weibull Predictions for the Ferrite Components - Gap (0.001 in.) Location

	Cycles to First Failure ("Cumulative Effect" Failure Free Time, yrs.)		Cycles to First Failure, "Cumulative Effect" (Failure Rate at End of Life, "Cumulative Effect")									
Component	Manufacturing [20°C … 80°C] Cyles to F = 10 ppm (n_i = 200 cycles)	Storage [17°C … 23°C] Cyles to F = 10 ppm (n_i = 3650 cycles)	Use Condition "B" [-10°C … 20°C] Cycles to F = 10 ppm (n_i = 5475 cycles)		Use Condition "C" [10°C … 40°C] Cycles to F = 10 ppm (n_i = 5475 cycles)		Use Condition "A" [20°C … 55°C] Cycles to F = 10 ppm (n_i = 5475 cycles)		Use Condition "D" [40°C … 70°C] Cycles to F = 10 ppm (n_i =5475 cycles)	
1806 #43 Material	928	299000	4499 (6.8)	3471 (19%)	2369 (5.0)	1828 (96%)	2053 (4.3)	1584 (99%)	2575 (5.4)	1987 (91%)
1806 #61 Material	1710	972500	10460 (25)	9192 (0%)	4446 (10.7)	3908 (15%)	2595 (6.2)	2281 (92%)	3588 (8.6)	3154 (46%)
1806 #73 Material	3057	918800	11010 (28)	10245 (0%)	6185 (15.7)	5755 (0%)	5323 (13.6)	4953 (1.1%)	6953 (17.7)	6470 (0%)

Table 17
Three-Parameter (3P) Weibull Predictions for the Ferrite Components - Fillet Location

	Cycles to First Failure ("Cumulative Effect" Failure Free Time, yrs.)		Cycles to First Failure, "Cumulative Effect" (Failure Rate at End of Life, "Cumulative Effect")									
Component	Manufacturing [20°C … 80°C] Cyles to F = 10 ppm (n_i = 200 cycles)	Storage [17°C … 23°C] Cyles to F = 10 ppm (n_i = 3650 cycles)	Use Condition "B" [-10°C … 20°C] Cycles to F = 10 ppm (n_i = 5475 cycles)		Use Condition "C" [10°C … 40°C] Cycles to F = 10 ppm (n_i = 5475 cycles)		Use Condition "A" [20°C … 55°C] Cycles to F = 10 ppm (n_i = 5475 cycles)		Use Condition "D" [40°C … 70°C] Cycles to F = 10 ppm (n_i =5475 cycles)	
0805 #43 Material	14310	897800	34730 (93)	34103 (0%)	31890 (86)	31314 (0%)	30210 (81)	29665 (0%)	42320 (114)	41556 (0%)
0805 #61 Material	17810	1500000	44640 (120)	44026 (0%)	41480 (112)	40910 (0%)	32740 (88)	32290 (0%)	49660 (134)	48977 (0%)
0805 #73 Material	24490	1500000	49740 (135)	49216 (0%)	51810 (140)	51264 (0%)	49570 (134)	49048 (0%)	73220 (198)	72448 (0%)
1206 #43 Material	13770	956000	34960 (94)	34318 (0%)	31000 (83)	30431 (0%)	29490 (79)	28949 (0%)	40930 (110)	40178 (0%)
1206 #61 Material	17820	1700000	47530 (128)	46892 (0%)	42050 (114)	41486 (0%)	32540 (88)	32103 (0%)	49220 (133)	48559 (0%)
1206 #73 Material	25430	1800000	52810 (143)	52285 (0%)	53480 (145)	52949 (0%)	51550 (140)	51037 (0%)	75800 (206)	75046 (0%)

Table 17 *(con't)*
Three-Parameter (3P) Weibull Predictions for the Ferrite Components - Fillet Location

	Cycles to First Failure ("Cumulative Effect" Failure Free Time, yrs.)		Cycles to First Failure, "Cumulative Effect" (Failure Rate at End of Life, "Cumulative Effect")							
Component	Manufacturing [20°C … 80°C] Cyles to F = 10 ppm (n_i = 200 cycles)	Storage [17°C … 23°C] Cyles to F = 10 ppm (n_i = 3650 cycles)	Use Condition "B" [-10°C … 20°C] Cycles to F = 10 ppm (n_i = 5475 cycles)		Use Condition "C" [10°C … 40°C] Cycles to F = 10 ppm (n_i = 5475 cycles)		Use Condition "A" [20°C … 55°C] Cycles to F = 10 ppm (n_i = 5475 cycles)		Use Condition "D" [40°C … 70°C] Cycles to F = 10 ppm (n_i =5475 cycles)	
1806 #43 Material	7526	410100	17390 (46)	16773 (0%)	16270 (43)	15693 (0%)	16150 (43)	15577 (0%)	22640 (60)	21836 (0%)
1806 #61 Material	9249	886600	23170 (62)	22573 (0%)	21640 (58)	21082 (0%)	17280 (46)	16835 (0%)	26700 (71)	26012 (0%)
1806 #73 Material	14200	887400	26750 (72)	26263 (0%)	28940 (77)	28143 (0%)	29570 (80)	29032 (0%)	44360 (119)	43552 (0%)

Table 18

Two-Parameter (2P) *and* Three Parameter (3P) Weibull Predictions for the Resistors and Capacitors - Gap (0.001 in.) and Fillet Locations *Accelerated Testing (0°C … 100°C)*

Failure Free Cycles … 3P Weibull *only* | **Cycles to the Failure Rate of 50% (Failure Rate at the End of Life, n_i = 2628 cycles)**

Component	2P Weibull Gap Location	3P Weibull Gap Location		2P Weibull Fillet Location	3P Weibull Fillet Location	
1206 Resistor	1769 (97%)	1153	1817 (98%)	25120 (83 ppm)	16370	25808 (0%)
2010 Resistor	414 (100%)	270	425 (100%)	77980 (0.90 ppm)	50820	80142 (0%)
2512 Resistor	387 (100%)	252	397 (100%)	91610 (0.47 ppm)	59700	94152 (0%)
1210 Capacitor	553 (100%)	360	568 (100%)	28060 (53 ppm)	18290	28837 (0%)
1812 Capacitor	234 (100%)	247	389 (100%)	23680 (110 ppm)	15430	24343 (0%)
1825 Capacitor	814 (100%)	530	836 (100%)	50110 (5.3 ppm)	32660	51503 (0%)

Table 19

Two-Parameter (2P) *and* Three Parameter (3P) Weibull Predictions for the Ferrite Components - Gap (0.001 in.) and Fillet Locations *Accelerated Testing (0°C … 100°C)*

	Failure Free Cycles … 3P Weibull *only*		Cycles to the Failure Rate of 50% (Failure Rate at the End of Life, n_i = 2628 cycles)		
Component	2P Weibull Gap Location	3P Weibull Gap Location		2P Weibull Fillet Location	3P Weibull Fillet Location	
0805 #43 Material	1374 (99%)	895	1411 (100%)	12040 (0.16%)	7848	14404 (0%)
0805 #61 Material	2707 (46%)	1764	2782 (38%)	15600 (560 ppm)	10170	16036 (0%)
0805 #73 Material	4362 (8.7%)	2843	4482 (0%)	20670 (180 ppm)	13470	21240 (0%)
1206 #43 Material	2838 (40%)	1849	2916 (29%)	11580 (0.18%)	7545	11900 (0%)
1206 #61 Material	6842 (1.5%)	4459	7031 (0%)	15850 (530 ppm)	10330	16289 (0%)
1206 #73 Material	10580 (0.26%)	6892	10868 (0%)	21620 (150 ppm)	14090	22216 (0%)

Table 19 *(con't)*

Two-Parameter (2P) *and* Three Parameter (3P) Weibull Predictions for the Ferrite Components - Gap (0.001 in.) and Fillet Locations *Accelerated Testing (0°C … 100°C)*

	Failure Free Cycles … 3P Weibull *only*		Cycles to the Failure Rate of 50% (Failure Rate at the End of Life, n_i = 2628 cycles)		
Component	2P Weibull Gap Location	3P Weibull Gap Location		2P Weibull Fillet Location	3P Weibull Fillet Location	
1806 #43 Material	895 (100%)	584	920 (100%)	6173 (2.3%)	4023	6344 (0%)
1806 #61 Material	2044 (85%)	1332	2100 (89%)	8005 (0.80%)	5217	8227 (0%)
1806 #73 Material	3332 (24%)	2172	3424 (7.2%)	11810 (0.17%)	7698	12135 (0%)